EVAPORATION FROM A FREE LIQUID SURFACE

AMAL LOTFI[1], JADRAN VRABEC[2] and JOHANN FISCHER[3]*

[1] *ista International GmbH, Grugaplatz 2, 45131 Essen, Germany*

[2] *Lehrstuhl für Thermodynamik und Energietechnik, Universität Paderborn, 33098 Paderborn, Germany*

[3] *Institut für Verfahrens- und Energietechnik, Universität für Bodenkultur, Muthgasse 107, 1190 Wien, Austria*

Abstract

Steady state evaporation from a planar liquid surface into vacuum is modelled by non-equilibrium molecular dynamics simulations of a Lennard-Jones fluid. Studies are made for liquids at a low temperature T/T_c = 0.53, a medium temperature T/T_c = 0.65 and a high temperature T/T_c = 0.84, where T_c is the critical temperature. Results are given for the profiles of density, kinetic temperature, distinguishing between its components, and drift velocity, for the outgoing, incoming and total particle flux as well as for the evaporation coefficient α. Moreover, velocity distribution functions are shown. The simulation results are compared with those from kinetic theory. The key findings are: a) For the low temperature, the simulations yield values for the vapour density and temperature as well as for the particle flux which confirm the assumption of Hertz about an outgoing half-sided Maxwellian which implies α = 1. b) For all temperatures, the density profiles do not change significantly in the liquid and in the interface in comparison with equilibrium. c) For the medium and high temperatures, the kinetic temperatures somewhat decrease already in the liquid and more in the interface which leads to a lower particle flux than assumed by Hertz and hence α decreases with temperature. Finally, a simple correlation is given to estimate α as a function of T/T_c.

Keywords: Evaporation into vacuum, Non-equilibrium molecular dynamics, Kinetic theory, Hertz model, Evaporation coefficient

*Corresponding author. Tel.: +43 676 47 55 349; Fax: +43-1-370 97 26-210

E-mail address: johann.fischer@boku.ac.at

Nomenclature

c	Sound velocity
f	Distribution function
H	Number of time steps divided by 10
J	Scaled particle flux
j	Particle flux
k_B	Boltzmann constant
Kn	Knudsen number
L	Edge length of the rectangular simulation volume
L_{vap}	Length of vapour phase
LJ	Lennard-Jones potential
LJR_c	Lennard-Jones potential cut and shifted at $R_c\sigma$
m	Molecular mass
M	Number of time steps
MD	Molecular dynamics
N	Number of particles
NEMD	Non-equilibrium molecular dynamics
p	Pressure
p_σ	Vapour pressure
q	Heat flux in kinetic theory
T	Temperature
T_c	Critical temperature
T_1	Liquid thermostat temperature
v	Velocity
x, y, z	Spatial coordinates
w	Width of liquid-vapour interface

Greek symbols

α	Evaporation (or condensation) coefficient
Δt	Time step
ΔV	Volume element
ε	Lennard-Jones energy parameter
λ	Mean free path
λ_H	Thermal conductivity
ρ	Density

σ	Lennard-Jones size parameter
τ	Time unit

Superscripts

H	Hertz
M	Maxwellian
D	Drift
E	Evaporated
0	Collisionless
*	Reduced quantity
+	Outgoing
–	Incoming
^	Contracted
´	Saturated liquid state
´´	Saturated vapour state

Subscripts

c	Critical point, Condensation
e	Evaporation
i, j	Numbering of volume elements
l	Liquid
le	Quantity in the liquid under steady state evaporation
tr	Triple point
v	Vapour
ve	Quantity in the vapour under steady state evaporation
x, y, z	Components in spatial *x*-, *y*-, *z*-direction

1. Introduction

Evaporation and condensation play an important role in natural and in technical processes. Nowadays, e.g. evaporative cooling or fuel droplet evaporation are applications of interest, where combined heat and mass transfer is the most challenging aspect. This topic can be approached by different theoretical methods: hydrodynamics, kinetic theory or molecular simulation. Early studies using the kinetic theory of gases were made by Hertz [1], Knudsen [2] and Volmer [3] assuming half-sided Maxwellian velocity distribution functions outgoing from and incoming to the liquid-vapour interface. In the late 1950s, problems like re-entry of spacecraft, switches for strong currents or laser-pellet fusion reinvigorated the interest in kinetic theory. Technically, the collision term in the Boltzmann equation was replaced by a simplified model collision term introduced by Welander [4] and Bhatnagar-Gross-Krook [5]. Initially, solutions were obtained from the linearized kinetic equation [6], later also strong evaporation was studied [7-9]. Whilst kinetic theory already captures essential physical features of evaporation and condensation, details concerning the vapour phase, the liquid-vapour interface and the liquid phase remained open and deserved more detailed studies. One crucial problem concerns the initial and the boundary conditions of the velocity distribution function.

When increasingly powerful computers became available, evaporation was studied by molecular dynamics (MD) which is thought to be the key methodology to validate the assumptions of kinetic theory. Thus molecular simulation data are available with respect to a) the dynamics of molecules at planar liquid-vapour interfaces under equilibrium [10-13], b) the injection of test particles into planar interfaces under equilibrium [14-16], c) the evaporation from planar surfaces by non-equilibrium molecular dynamics (NEMD) [17-23] and d) the evaporation from droplets [24-32] or fluid bridges in a pore [33] by NEMD. Here, we

concentrate on planar surfaces because they are more suited to represent evaporation in macroscopic systems than nano-scaled droplets.

One important item for all interfacial studies and hence also for evaporation is the cut-off scheme that is applied to the intermolecular potential. Being the most prominent example, we consider Lennard-Jones (LJ) type potentials that have the energy parameter ε and the size parameter σ. In the following all quantities are reduced by ε and σ, e.g. temperature $T^* = k_B T/\varepsilon$, with k_B being Boltzmann's constant, or density $\rho^* = \rho\sigma^3$, and the asterisk is omitted if no confusion can occur. The LJ potential exhibits attractive forces up to large distances, but in MD simulations the interaction between two molecules can be explicitly evaluated only up to some distance R_c using e.g. a truncated and shifted potential. If the long range forces are neglected, the fluid is termed LJR_c fluid here. Alternatively, appropriate long range corrections may be used so that results are obtained for the fluid with the full LJ interactions, which is termed LJ fluid. Whilst these corrections are standard for homogeneous fluids, they were worked out for MD of inhomogeneous fluids in Ref. [34], where also the effects of different cut-off radii (up to $R_c = 5.0$) and of different correction schemes were discussed. The differences between the properties of the LJ fluid and the LJR_c fluids are caused by the fact that the truncation as well as the shift of the LJ potential act as a reduction of the attractive potential. Hence, the critical temperature in terms of ε/k_B decreases, which results in a significant increase of the saturated vapour density at a given value of $k_B T/\varepsilon$, which is important for evaporation studies.

For the LJ fluid, vapour-liquid equilibria were calculated via the equality of the chemical potential with the NpT + test particle method [35], yielding a critical temperature $T_{cLJ} = 1.31$. These phase equilibrium results were used to develop accurate equations of state for the LJ

fluid [36-38]. Vapour-liquid equilibria were also studied by direct simulations [17, 34, 39], which yielded orthobaric densities that are in very good agreement with the results from the NpT + test particle method [35]. Estimates for the triple point temperature T_{tLJ} of the LJ fluid are compiled in [40] and scatter between 0.661 and 0.698, another source [41] reports T_{tLJ} = 0.694.

Vapour-liquid equilibria were also investigated for LJR_c fluids. First, van Megen and Snook [42] found for LJ2.5 $T_{cLJ2.5}$ = 1.12. A series of other papers followed considering R_c = 2.5 and other cut-off radii, of which we mention only a few here. For the LJ2.5 fluid, Smit [43] found $T_{cLJ2.5}$ = 1.085 ± 0.005 and Vrabec et al. [44] found $T_{cLJ2.5}$ = 1.0779. Assuming for simplicity an average value of $T_{cLJ2.5}$ = 1.08 for the LJ2.5 fluid, we see that $T_{cLJ2.5}/T_{cLJ}$ = 0.82. For the LJ3.5 fluid, Anisimov et al. [19] found $T_{cLJ3.5}$ = 1.21, and for the LJ5.0 fluid, Panagiotopoulos [45] obtained $T_{cLJ5.0}$ = 1.28. As the critical temperature k_BT_c/ε decreases with decreasing R_c, the saturated vapour densities $\rho''\sigma^3$ increase significantly at the same reduced temperature k_BT/ε. E.g., for LJ2.5 it increases by a factor of about 3(!) [34, 44]. Unfortunately, it is frequently ignored by researchers in NEMD that the properties of LJR_c fluids very much differ in units reduced by ε and σ, depending on the cut off radius R_c. This causes problems in assessing results which was already pointed out in Ref. [27] for droplet evaporation and will be encountered below again for evaporation from a planar surface. In the comparisons below, we tried to account for these differences.

Let us turn now to the MD evaporation studies for planar surfaces. In Refs. [10-13] classifications of particle trajectories were made giving insights into the particle dynamics in the interface under equilibrium. The work of Matsumoto et al. [11, 12] was extended by Tsuruta et al. [14-15] by injecting test particles from the vapour side onto the interface region

under equilibrium. With this methodology they obtained condensation and evaporation coefficients and also velocity distribution functions of evaporated and reflected molecules. In subsequent work, Tsuruta et al. combined their methodology with transition state theory [16].

Extensive NEMD studies on steady state evaporation from the planar surface of a thermostated liquid have been made - to the best of our knowledge – for the first time in the PhD thesis of Lotfi [17]. He performed NEMD simulations for the full LJ potential using R_c = 5.0 and the long range correction LRC2 from Ref. [34]. Systems with N = 1372 particles were considered at the three temperatures T/T_{cLJ} = 0.53, 0.65 and 0.84, where T is the bulk liquid temperature.

The two papers by Anisimov et al. [18, 19] on evaporation of LJR_c fluids into vacuum are somewhat overlapping. In the second paper the cut-off radius was R_c = 3.5, no long range corrections were made and the particle number was N = 12,000. Ref. [19] gives $T_{cLJ3.5}$ = 1.21 and hence the range of reduced liquid temperatures T/T_c considered was between 0.615 and 0.80. The results contain profiles of density, parallel and perpendicular temperature, drift velocity as well as particle fluxes, and also velocity distribution functions. Moreover, Anisimov et al. discussed the interface thickness and surface tension and gave values for the evaporation coefficient α.

Next, a related study was made by Ishiyama et al. [20] for the LJ4.4 fluid. We estimate $T_{cLJ4.4}$ = 1.25 based on Refs. [19, 45] and the argon parameters used by authors. They performed calculations with N = 2000 particles in the temperature range $0.57 < T/T_c < 0.67$ and with N = 4000 for $0.73 < T/T_c < 0.87$. For the temperature T/T_c = 0.53 and two lower temperatures, however, the authors used an other potential than LJ4.4. Results of the same type as obtained by Lotfi [17] and by Anisimov et al. [18, 19] were reported.

NEMD simulations for evaporation of the LJ2.5 fluid into vacuum were made by Hołyst and Litniewski [21] with much larger particle numbers N = 800,000 in the temperature range $T_l/T_{cLJ2.5}$ between 0.65 and 0.79. The authors considered steady state evaporation from a thermostated liquid similar to Refs. [17-20] and transient evaporation from a liquid without energy supply which corresponds to adiabatic pressure jump evaporation [27]. The most interesting feature was the introduction of a pseudo-temperature T_{out}, corresponding to the kinetic energy of the vapour during evaporation and their finding that the equilibrium vapour pressure $p_\sigma(T_{out})$ is approximately equal to the liquid pressure p_l during steady state evaporation into vacuum.

With time progressing the number of particles further increased in the paper by Cheng et al. [22] to N = 3,000,000, who studied transient evaporation. The considered temperature range from $T_l/T_{cLJ2.5}$ = 0.74 to 0.92 was higher than in all earlier papers. The physics of Ref. [22], however, suffers from the fact that the difference between the full LJ fluid and the LJ2.5 fluid has been ignored. Some problems of this mix-up for evaporation studies were already pointed out in Ref. [27]. It also seems to be the cause for some findings in Ref. [22] and for the statement "However, it is well known that the vapour pressure of a LJ fluid is much higher than those of real liquids", which contradicts with reliable results for Ar, Kr, Xe and methane in Ref. [46] and several earlier sources cited therein. Moreover, it is known that these real fluids can also be modelled with a good accuracy as LJ2.5 fluids with, however, different values for ε and σ than for the LJ fluid [44].

To our knowledge, the most recent simulation study on evaporation from a planar liquid surface is that of Yu and Wang [23], who considered three-phase systems consisting of two solid walls at different temperatures with adjacent liquid films and transient evaporation from the hot to the cold side. The authors used N = 9,300 particles and a LJ potential truncated at

167 3.5σ without switching or shifting. This complex study gives interesting hints for discussing
168 theories and experiments [47-52].

169 From the above mentioned papers on NEMD simulations for evaporation from a planar
170 liquid surface [17-23], the pioneering work of Lotfi [17] was rarely and only recently
171 recognized [9, 32], presumably because it appeared as a PhD thesis in German language. The
172 unique features of Ref. [17] are: 1) the consideration of the full LJ fluid and 2) the
173 investigation of evaporation at the reduced temperature T/T_{cLJ} = 0.53, which is by far the
174 lowest temperature of all studies on LJ type fluids. The merit of these features as well as the
175 separation of the outgoing and incoming fluxes is that the assumptions of Hertz [1] and
176 Knudsen [2] for low pressure evaporation can be discussed in more detail. Hence, we present
177 here the most important simulation results for evaporation into vacuum from the original
178 work [17] accompanied by a discussion of new aspects. Because of the large extent of the
179 data on evaporation into vacuum provided in [17], part of it is given in the Supplementary
180 Material. The results on evaporation at some counter-pressure given in [17] shall be presented
181 in a subsequent publication.

182 The present paper is organized such that in Sec. 2 some assumptions and results of kinetic
183 theory are compiled which are required later for comparisons with MD results. In Sec. 3 the
184 simulation methodology is described and in Sec. 4 results are given and discussed. In Sec. 5
185 we compare results of different authors for the evaporation coefficient α of LJ type fluids and
186 present a simple correlation for the evaporation coefficient as a function of the temperature
187 for the fluid with the full LJ interaction.

2. Assumptions of kinetic theory

According to kinetic theory, a gas is described by the distribution function f depending on the spatial coordinate vector $r = (x, y, z)$, the velocity coordinate vector $v = (v_x, v_y, v_z)$ and the time t, $f = f(r, v, t)$. The normalization is chosen such that integration of f over the velocities yields the density $\rho\,(r, t)$

$$\rho\,(\mathbf{r},\ t) = \int f(\mathbf{r}, \mathbf{v}, t)\, d\mathbf{v}\,. \tag{1}$$

Quantities of interest are the drift velocity $\mathbf{v}^D(\mathbf{r}, t)$, the particle flux $\mathbf{j}(\mathbf{r}, t)$, and the kinetic temperature $T(\mathbf{r}, t)$ as well as its components such as $T_z\,(\mathbf{r}, t)$. These are obtained from the distribution function f as

$$\mathbf{j}(\mathbf{r}, t) = \rho\,(\mathbf{r},\ t)\,\mathbf{v}^D(\mathbf{r}, t) = \int \mathbf{v}\, f(\mathbf{r}, \mathbf{v}, t)\, d\mathbf{v}\,, \tag{2}$$

and

$$\rho\,(\mathbf{r}, t)\, k_B T_z\,(\mathbf{r}, t) = (m/3) \int (v_z - v_z^D)^2\, f(\mathbf{r}, \mathbf{v}, t)\, d\mathbf{v}\,, \tag{3}$$

with m being the molecular mass. Analogous equations hold for $T_x\,(\mathbf{r}, t)$ and $T_y\,(\mathbf{r}, t)$ and the total temperature $T(\mathbf{r}, t)$ is given as the average

$$T(\mathbf{r}, t) = (1/3)\,[T_x\,(\mathbf{r}, t) + T_y\,(\mathbf{r}, t) + T_z\,(\mathbf{r}, t)]. \tag{4}$$

For systems under equilibrium it is well known that the distribution function f becomes the Maxwellian function

$$f^M = \rho\,(m/2\pi k_B T)^{3/2} \exp\{-(m/2k_B T)\mathbf{v}^2\}, \tag{5}$$

and that the mean free path λ is given as

$$\lambda = 1/(2^{1/2}\,\pi\,\rho\,\sigma^2), \tag{6}$$

where it is assumed for simplicity that the molecular diameter is the LJ size parameter σ. Moreover, if a flow with a drift velocity $\boldsymbol{v}^D$ is in its steady state, the distribution function f tends again towards a Maxwellian with respect to the drift velocity

$$f^M = \rho\,(m/2\pi kT)^{3/2} \exp\{-(m/2kT)(\boldsymbol{v} - \boldsymbol{v}^D)^2\}. \tag{7}$$

For a planar geometry, which depends only on the z-direction under steady state flow conditions, the distribution function reduces to $f = f(z, v_x, v_y, v_z)$. In this case it is helpful to introduce a contracted distribution function

$$\hat{f}_z(z, v_z) = (1/\rho)\int f(z, v_x, v_y, v_z)\, dv_x dv_y, \tag{8}$$

which is normalized to unity.

Let us consider a fictitious plane at $z = 0$ in a gas under equilibrium. Then the particle flux j^+ through the plane from $z < 0$ to $z > 0$ is determined via Eq. (2) by using a half-sided Maxwellian f^+ defined as

$$f^+ = \rho\,(m/2\pi k_B T)^{3/2} \exp\{-(m/2k_B T)\boldsymbol{v}^2\} \quad \text{for } v_z > 0\,, \tag{9a}$$

$$f^+ = 0 \quad \text{for } v_z < 0\,. \tag{9b}$$

Next, we consider a planar liquid surface at $z = 0$. The liquid is kept at a constant temperature T_1 and evaporates under steady state conditions into positive z-direction. For that situation, Hertz [1] assumed that the evaporating particles have a half-sided Maxwellian distribution f^+ given by Eqs. (9a) and (9b) with $T = T_1$ and $\rho = \rho''$ being the saturated vapour density at T_1. For the outgoing vapour, the following results are obtained from Eqs. (1) to (4) [8]

$$\rho^{+H} = 0.5\,\rho'', \tag{10}$$

$$j^{+H} = \rho''(k_B T_1 / 2\pi m)^{1/2}, \quad (11)$$

$$T^{+H} = [(3\pi - 2)/3\pi]\, T_1, \quad (12)$$

$$T_{xy}^{+H} = T_1, \quad (13)$$

$$T_z^{+H} = (1 - 2/\pi)\, T_1. \quad (14)$$

Regarding the incoming particle flux j^-, a simple concept assumes a half-sided Maxwellian f^- with the temperature T_2 and the density ρ_2 of the gas. The half-sided Maxwellians f^+ and f^- are shown in contracted form in Fig. 1. The resulting flux of condensing particles is given by the incoming Hertz flux j^{-H}

$$j^{-H} = \rho_2 (k_B T_2 / 2\pi m)^{1/2}, \quad (15)$$

and hence the total flux from the surface is

$$j = j^{+H} - j^{-H} = \rho'' (k_B T_1 / 2\pi m)^{1/2} - \rho_2 (k_B T_2 / 2\pi m)^{1/2}. \quad (16)$$

Because of discrepancies with his experiments, Knudsen [2] introduced an evaporation coefficient α_e and a condensation coefficient α_c and modified the total flux to

$$j = \alpha_e j^{+H} - \alpha_c j^{-H}. \quad (17)$$

For a more sophisticated treatment of evaporation by kinetic theory, the Boltzmann equation with the Boltzmann-Bhatnagar-Gross-Krook-Welander (BBGKW) collision term [4, 5] was used [6-8]. The crucial point, however, are the boundary conditions for *f*. An interesting result of Ref. [8] for evaporation into vacuum is that about 15% of the evaporated particles are backscattered to the surface. Moreover, the temperature and the density decrease with increasing distance *z* from the surface. Because the total particle flux *j* in the steady state

is constant, this implies according to Eq. (2) that with decreasing vapour density ρ, the drift velocity v_z^D has to increase with z.

The question is now which assumptions can be clarified with NEMD simulations. For the outgoing particles, it can be investigated whether their distribution function is a half-sided Maxwellian with the liquid temperature T_1 and the saturated vapour density ρ''. The question about the distribution function of the incoming particles for evaporation into vacuum is more subtle and depends on the Knudsen number Kn, which is the ratio of the mean free path λ in the vapour phase to the length L_v of the vapour volume in z-direction

$$\mathrm{Kn} = \lambda / L_v. \tag{18}$$

Obviously, several collisions per particle are necessary to obtain an "equilibrated flow" as described by Eq. (7), which means that small Knudsen numbers [8] are required for assessing the incoming distribution function.

3. Simulation methodology

Steady state evaporation of a LJ fluid from a planar liquid surface into vacuum was studied with N = 1372 molecules. The cut-off radius for the explicit evaluation of particle-particle forces was 5σ and long-range force corrections were made as described in Ref. [34] as LRC2 by using averaged density profiles. All quantities are given in units reduced by ε and σ as stated above and the time step in the simulations was $\Delta t = 0.005\ \tau$, with $\tau = \sigma(m/\varepsilon)^{1/2}$ being the usual time unit. The equations of motion were solved with the fifth order predictor-corrector algorithm [53, 54].

In the first step, vapour-liquid equilibrium configurations were created as described in [34]. The system containing N particles was started from a lattice configuration in a

rectangular volume of dimension L_x x L_y x $L_{z,0}$ with $L_x = L_y$ and $L_{z,0} = 1.5L_x$. An equilibration run was made with usual periodic boundary conditions and the minimum image convention to obtain a liquid configuration. Subsequently, the periodic boundary conditions were removed in the *z*-direction and the simulation volume was enlarged to a value of $L_z = 3L_{z,0} = 4.5L_x$ with reflecting walls on both sides. After another equilibration period, production runs were made for the liquid slab with vapour phases on both sides over 25,000 time steps for $T_1 = 0.70$ ($T_1/T_c = 0.53$), $T_1 = 0.85$ ($T_1/T_c = 0.65$) and $T_1 = 1.10$ ($T_1/T_c = 0.84$).

Next, evaporation into vacuum was initiated by replacing the reflecting walls with virtual planes and removing all particles from the vapour which cross these planes. For obtaining steady state evaporation two actions were taken: 1) The temperature T_1 was kept constant by momentum scaling in the central region of the liquid film with a width of 4σ, cf. black marked area in Fig. 2.2) The removed particles were reinserted into the centre of the liquid film, cf. arrows in Fig. 2. Reinserted particles kept their spatial *x*- and *y*-coordinate and were assigned with a random velocity. In order to minimize overlaps with other particles in the liquid during reinsertion, initially a small molecular size and a repulsive potential were assumed. Then, similar as in Ref. [55], the reinserted particles grew gradually and when they reached their full size after 100 time steps, the attractive interaction was switched on. With this procedure only 1 to 2 particles were simultaneously in their growth phase. Sampling for the steady state flow was started after a flow equilibration period of at least 5,000 time steps and the production runs lasted over *M* time steps, with *M* ranging from 30,000 to 150,000.

A technical problem was the drift of the liquid slab because momentum conservation was violated by the removal and reinsertion of particles and by thermostating the centre of the liquid slab. On average, these momenta should cancel out, but they actually lead to small

displacements of the liquid slab of 2 to 4σ in the one or the other direction during the longer simulation runs. Because the thickness of the slab remained constant, we performed block averages over 5,000 time steps with subsequent centering of the liquid. For a further increase of the accuracy, the nearly symmetric profiles of all data were cut in the centre and superimposed so that results are presented here only for one averaged surface.

In order to see how the steady state evaporation into vacuum develops with increasing distance from the surface, we performed in addition to the simulations with an edge length $L_z = 3L_{z,0} = 4.5L_x$ also simulations with $L_z = 5L_{z,0} = 7.5L_x$.

For sampling steady state evaporation, the simulation volume was subdivided into volume elements ΔV with a thickness $\Delta z = L_z/100$, yielding $\Delta V = L_x L_y \Delta z$ and after each 10^{th} time step all quantities were stored. Hence, for M time steps the number of sampled data for each volume element and each quantity amounted to $H = M/10$. Let N_i be the cumulated number of particles counted in a volume element at position z_i during the whole run, then the local number density is

$$\rho_i = \frac{N_i}{\Delta V \cdot H} \quad . \tag{19}$$

The drift velocity in z-direction at the distance z_i was obtained by averaging the z-component of the particle velocities in the corresponding volume element

$$v_{z\,i}^{D} = \left\langle v_z \right\rangle_i = \frac{1}{N_i} \sum_{j=1}^{N_i} v_{z\,i,j} \quad . \tag{20}$$

The x, y and z-components of the kinetic temperatures T_x, T_y and T_z at the distance z_i were calculated by averaging over the kinetic energy contributions relative to the drift velocity as

$$k_B T_{xi} = m\left\langle v_x^2 \right\rangle_i = \frac{m}{N_i}\sum_{j=1}^{N_i} v_{x\,i,j}^2 \quad , \tag{21}$$

and analogously for $k_B T_{yi}$, whilst

$$k_B T_{z\,i} = m\left[\left\langle v_z^2 \right\rangle_i - \left\langle v_z \right\rangle_i^2\right] = \frac{m}{N_i}\sum_{j=1}^{N_i} v_{z\,i,j}^2 - m\left(v_z^D\right)_i^2 \ . \tag{22}$$

Because T_x and T_y should be identical, a temperature parallel to the surface T_{xy} may be introduced as a mean quantity of T_x and T_y at z_i

$$T_{xyi} = \frac{1}{2}(T_{xi} + T_{yi}), \tag{23}$$

and the total kinetic temperature T as a mean quantity of all three temperature components at z_i

$$T_i = \frac{1}{3}(T_{xi} + T_{yi} + T_{zi}). \tag{24}$$

The evaporating particle flux j_z can be obtained from the number of particles N_e which leave the simulation volume in M time steps of length Δt

$$j_z^E = \frac{N_e}{L_x \cdot L_y \cdot M \cdot \Delta t} \quad , \tag{25}$$

or alternatively, j_z can be obtained as a product of the density and the drift velocity

$$j_z^D = \rho_i \ v_{z\,i}^D \, , \tag{26}$$

which should be constant under steady state evaporation at any distance z_i. Moreover, the particle flux j_z is the superposition of the flux away from the surface $j_z^+{}_i$ and of the flux towards the surface $j_z^-{}_i$. Both can be determined similarly as in Eq. (25) and may, contrary to the total particle flux j_z, depend on the position z_i.

Next, kinetic theory [6] also considers a heat flux in z-direction q_{zi} that is defined as

$$q_{zi} = \frac{m}{2}\rho_i \cdot \left\langle \left[v_x^2 + v_y^2 + \left(v_z - v_z^D\right)^2 \right] \left(v_z - v_z^D\right) \right\rangle_i \quad , \tag{27}$$

which requires averages over the cubic quantities $\left\langle v_x^2 v_z \right\rangle_i$, $\left\langle v_y^2 v_z \right\rangle_i$ and $\left\langle v_z^3 \right\rangle_i$ that are calculated in analogy with the averages in Eqs. (21) and (22).

Finally, we were also interested in the contracted velocity distribution function $\hat{f}_z(z, v_z)$ as introduced in Eq. (10). It was determined by counting the number of particles $N_{zk,i}$ which are both in the volume element Δz at z_i and in the velocity element Δv_z at v_{zk}, where normalization to unity was obtained as

$$\hat{f}_z(z_i, v_{zk}) = \frac{N_{zk,i}}{N_i} . \tag{28}$$

4. Results and Discussion

NEMD simulations were made for the three temperatures T_1 = 0.70, 0.85 and 1.10. At each temperature, three runs were carried out using different edge lengths L_z or different numbers of time steps M. As an overview, Table 1 presents the simulation parameters, auxiliary data and key results for all nine runs. For quantities that change in the direction of evaporation flow, the key results in Table 1 refer to the bulk of the liquid or to the "bulk" of the vapour. The latter was chosen with some arbitrariness because the density, the temperatures and the drift velocity vary within the vapour.

Table 1 gives in addition to the number of sampled time steps M the following quantities: the thermostat temperature T_l, the edge length of the volume in z-direction L_z, the edge length of the volume in x-direction L_x with $L_y = L_x$, the temperature of the liquid under steady state evaporation T_{le}, the saturated liquid density ρ' at T_1, the density of the liquid under steady

state evaporation ρ_{le}, the drift velocity of the liquid under steady state evaporation $v_{z,le}^{D}$, the temperature of the vapour under steady state evaporation T_{ve}, the x, y- and z-components of the temperature of the vapour under steady state evaporation $T_{xy,ve}$ and $T_{z,ve}$, the saturated vapour density ρ'' at T_1, the density of the vapour under steady state evaporation ρ_{ve}, the mean free path in the vapour $\lambda = 1/(2^{1/2}\pi\rho_{ve})$, the drift velocity of the vapour under steady state evaporation $v_{z,ve}^{D}$, the particle flux j_z^E determined via Eq. (25) from the number of evaporated particles, the particle flux j_z^D determined by using the drift velocity and Eq. (26), the outgoing Hertz flux $j_z^{+H} = \rho''(T_1/2\pi)^{1/2}$ of the vapour under equilibrium, the evaporation coefficient $\alpha = j_z^E / j_z^{+H}$ and the sound velocity of the ideal gas $c = (\kappa T_{ve})^{1/2}$ with $\kappa = 5/3$.

The auxiliary parameters in Table 1, the orthobaric densities ρ' and ρ'' and the outgoing Hertz flux j_z^{+H}, were taken or calculated from the data in Ref. [35].

More details including spatial profiles for quantities which change from the liquid through the interface to the vapour, like density or temperature, and the velocity distribution functions as well as discussions of the results will be given for each of the three temperatures T_1 in the following subsections. Note that in the figures the z-direction extends only to $L_z/2$, because the nearly symmetric profiles resulting from the geometry of Fig. 2 were cut in the centre, superimposed and averaged. Hence, the length of the vapour volume L_v extended from about z = 10 up to $L_z/2$ and is accordingly given as $L_v = L_z/2 - 10$. Moreover, the interface is understood as the region in which the density changes from ρ_{le} to ρ_{ve} and its width w was determined via an intersection of the tangent to $\rho(z)$ at the point of inflection with ρ_{le} and ρ_{ve}.

The evaporation coefficient merits a dedicated discussion. In kinetic theory, the evaporation coefficient α_e is defined as the ratio of the flux outgoing from a mathematical

surface to the Hertz flux $\alpha_e = j_z^+ / j_z^{+H}$. However, if the model is refined from the kinetic length scale to the molecular length scale, the interface is not a mathematical plane any more, but a finite film in which the thermophysical quantities vary. Then the question arises at which plane the outgoing flux has to be taken and how the outgoing flux has to be separated from the incoming flux. Because it seems difficult to clarify this issue without ambiguity, we decided for the sake of simplicity to define the evaporation coefficient α as

$$\alpha = j_z^E / j_z^{+H} \quad , \tag{29}$$

where j_z^E is the total particle flux for evaporation into vacuum. Because $j_z^E = j_z^+ - j_z^-$, α is smaller than α_e and the difference depends on the flux j_z^- of backscattered particles. We note that the backscattered flux a) increases with the length of the vapour volume L_v and b) increases when approaching the surface. It should be reminded that the maximum backscattered flux occurs for evaporation in case of $L_v \to \infty$ and was found to be about 15% [8]. With this background, we took in the following subsections the total particle flux j_z^E for the shorter vapour volume L_v and considered the backscattered flux for the longer vapour space L_v to estimate the maximum uncertainty of the evaporation coefficient α as defined by Eq. (29).

In order to link the LJ model to a real fluid we consider methane as a reference [56], because it can be accurately described by the LJ potential [46].

4.1. Evaporation at low temperature

The low temperature T_1 = 0.70 is equivalent to T_1/T_c= 0.534. For methane $0.534T_c$ = 101.46 K, where the vapour pressure is 0.41 bar.

As seen from Table 1 three simulation runs were made. Runs 1 and 2 were carried out independently, but with the same L_z = 46 while M was increased from 100,000 and 120,000. In Run 3, the length L_z was extended from 46 to 77 and M increased to 150,000. The corresponding lengths of the vapour volume were L_v = 13.1 for Runs 1 and 2 and L_v = 28.6 for Run 3. Comparing the results for all three runs given in Table 1, it can be seen that all temperatures agree well and the same holds for the liquid density. A reasonable agreement was also obtained for the drift velocities in the vapour and for the particle fluxes j_z^E and j_z^D determined by both methods. Regarding the expected strong scattering of the liquid drift velocity, a test calculation via $v_{z,lev}^D = j_z / \rho'$ with an averaged value for j_z = 0.00072 yielded $v_{z,lev}^D$ = 0.0006, which confirms the qualitative correctness of the directly calculated quantities. Less satisfying is the disagreement of the vapour density from Runs 1 and 2 on the one side and from Run 3 on the other side, which, however, is within the combined (large) statistical uncertainties for these small values, cf. Ref. [35].

Spatial profiles of the density $\rho(z)$, the temperatures $T_{xy}(z)$ and $T_z(z)$ and for the drift velocity $v_z^D(z)$ extending from the liquid through the interface into the vapour from Run 3 are shown in Fig. 3. The corresponding profiles from Run 1 are given in Fig. S1 of the Supplementary Material.

Considering the results given in Table 1 and Fig. 3, it can be seen that during steady state evaporation, the temperature T_{le} and the density ρ_{le} in the liquid are practically the same as under equilibrium conditions. In the interface, the shape of the density profile $\rho(z)$ and its width w = 1.75 remain also nearly the same as under equilibrium conditions [34, 39]. Large differences with respect to the equilibrium occured, as expected, in the vapour phase. The

vapour density averaged over the three runs is only ρ_{ve} = 0.0011, which is about the half of the saturated vapour density ρ´´ = 0.00207. The averaged temperature parallel to the surface $T_{xy,ve}$ = 0.65 is slightly lower than T_1 = 0.70 and shows maxima up to 0.75, the averaged temperature in flow direction is $T_{z,ve}$ = 0.30 and shows minima down to 0.26 and the averaged total temperature is T_{ve} = 0.54. The particle fluxes j_z^E and j_z^D are all around 0.69, with the exception of j_z^D from Run 3, which is higher due to the higher value of ρ_{ve}. The averaged drift velocity is $v_{z,ve}^D$ = 0.67 and increases in Run 3 with z up to $v_{z,ve,\max}^D$ = 0.75, cf. Fig. 3. Finally, the sound velocity $c = (\kappa T)^{1/2}$ calculated with κ =5/3 and $T = T_{ve}$ is c= 0.95, and hence the ratio of the maximum drift velocity to the sound velocity is $v_{z,ve,\max}^D / c$ = 0.79.

For a further discussion, we note that the vapour volume had a length of L_v = 13.1 for Runs 1 and 2 and L_v = 28.6 for Run 3. Since the mean free path λ varied from 225 for Run 1 and 2 to 173 for Run 3, the Knudsen number varied from Kn = 17 for Runs 1 and 2 to Kn = 6 for Run 3, which means that the simulations came very close to a collisionless flow in the vapour.

In Run 3, the particle flux j_z^D was also separated into the outgoing particle flux j_z^+ and the incoming particle flux j_z^-. The results are shown in Fig. 4, where a scaling by the Hertz flux at the local density $\rho(z)$ and the temperature T_1 was made according to $J_z^+ = j_z^+ / [\rho(z)(T_1/2\pi)]$ to bring the results for the liquid and the vapour into one scale. In the liquid, the fluxes J_z^+ and J_z^- were nearly the same. However, in the vapour at the distance z = 20, the outgoing flux was J_z^+ = 2 while the incoming flux was J_z^- = 0.07, which means that 3.5 % of the evaporated particles were backscattered by collisions. This is in qualitative agreement with the findings in Ref. [8], from which the backscattered flux for Kn = 10 was estimated to be 2%.

Because Runs 1 to 3 are NEMD simulations for nearly collisionless flow, they may be used to check the assumption of Hertz [1] that evaporating particles have a half-sided Maxwellian distribution f^+ with a temperature T_1 and a density ρ''. This check can be made for f^+ directly but also for its moments ρ^{+H}, j^{+H}, T^{+H}, T_{xy}^{+H} and T_z^{+H} as given by Eqs. (10) to (14). Considering the results from Runs 1 and 2, which are closer to the collisionless case than Run 3 because of their smaller vapour volume length L_v, cf. Table 1, we get $\rho_{ve}/\rho^{+H} = 0.97$, $\alpha = j_z^E / j_z^{+H} = 1.01$, $T_{ve}/ T^{+H} = 0.96$, $T_{xy,ve}/T_{xy}^{+H} = 0.92$ and $T_{z,vev}/ T_z^{+H} = 1.18$. Hence, it can be seen that the assumption of Hertz for the evaporated flux is confirmed by the present simulation data within their uncertainty for the vapour density ρ, the total kinetic temperature T and the particle flux j. Regarding the components of the kinetic temperature T_{xy} and T_z, it can be seen that the simulation data for the component parallel to the surface T_{xy} was 8% lower, whereas the component in flow direction T_z was 18% higher than the assumptions of kinetic theory. Because T_{xy} and T_z change from the liquid to the vapour only in the outermost region of the interface, a possible explanation for these deviations from the Hertz model could be that the few collisions in that region have the tendency to reduce the difference between T_{xy} and T_z.

Moreover, Fig. 5 shows contracted velocity distribution functions $\hat{f}_z$ in the liquid and the vapour sampled either directly from the simulations or obtained as Maxwellians according to Eq. (7) with temperatures and drift velocities for the liquid and the vapour from Table 1. In the liquid, the directly sampled values match very well with the Maxwellian. In the vapour, the directly sampled values exhibit large statistical uncertainties due to the small number of particles. Nevertheless, a distribution function consisting of two half-sided Maxwellians as

assumed by Hertz and as shown in Fig. 1 seems to better coincide with the directly sampled values than a single Maxwellian with a drift velocity according to Eq. (7).

Finally, we address the temperature increase in the vapour close to the liquid during evaporation of water at $T/T_c = 0.43$ found by Ward and Stanga [51]. In our understanding they did not measure the kinetic temperature but rather the temperature equivalent of the kinetic energy. Our data given in Table 1, however, show that the kinetic energy at $T/T_c = 0.53$ remains nearly the same in going from the liquid to the vapour. Hence, the temperature increase for water found in Ref. [51] can not be explained on the molecular scale by the LJ fluid.

4.2. Evaporation at medium temperature

The medium temperature $T_1 = 0.85$ is equivalent to $T_1/T_c = 0.649$. For methane at $0.649T_c$ = 123.73 K, the vapour pressure is 2.47 bar and is hence six times higher than in case of the low temperature $T_1 = 0.70$.

At $T_1 = 0.85$, Runs 4 and 5 were carried out with $L_z = 47.3$ and Run 6 with $L_z = 78.8$, cf. Table 1. Hence, the length of the vapour volume was $L_v = 13.6$ for Runs 4 and 5, whereas L_v = 29.4 for Run 6. The mean free path λ in the vapour varied from 53 for Runs 4 and 5 to 63 for Run 6, which means that Kn = $\lambda/L_v = 3.9$ for Runs 4 and 5 and Kn = 2.1 for Run 6. These conditions do not correspond to collisionless flow, but the number of collisions was still small. In Runs 4 and 5 only every fourth particle and in Run 6 every second particle underwent a collision in the vapour phase. The number of time steps M was 100,000 for Run 4, and 75,000 for Runs 5 and 6. Comparing the results from Runs 4 to 6 in Table 1, it can be seen again that the drift velocities in the liquid $v_{z,le}^{D}$ and the density in the vapour ρ_{ve} exhibit a stronger scatter.

Profiles for the density $\rho(z)$, the temperatures $T_{xy}(z)$ and $T_z(z)$ and for the drift velocity $v_z^D(z)$ from Run 6 are shown in Fig. 6. The corresponding profiles for Run 4 are given in Fig. S2 of the Supplementary Material. Considering the results in Table 1 and Fig. 6, a similar behaviour was found for the density as in the low temperature case with a somewhat broader interfacial width $w = 2.1$ and an average value of ρ_{ev} which is 16% lower than ρ^{+H}.

More interesting are the temperature profiles for T_{xy} and T_z, which decrease already slightly in the liquid, stronger in the interface and at the beginning of the vapour and continue to decrease in the bulk of the vapour. Considering the averaged vapour temperatures from Runs 4 and 5 in comparison with the Hertz values being $T^{+H} = 0.67$, $T_{xy}^{+H} = 0.85$ and $T_z^{+H} = 0.30$, it can be seen that T_{ve} is lower by 7%, $T_{xy,ve}$ is lower by 13% and $T_{z,ve}$ is higher by 28%. The fact that the temperature $T_{xy,ve}$ averaged from Runs 4 and 5 is 10% higher than that from Run 6 and that $T_{z,ve}$ from Runs 4 and 5 is 13% lower than that from Run 6 is an effect of the larger number of collisions due to the longer vapour volume L_v in Run 6.

The particle fluxes j_z^E and j_z^D are all around 0.31, with the exception of j_z^D from Run 6 which is lower due to ρ_{ve}. In Run 6, the particle flux j_z^D was separated into j_z^+ and j_z^- and the rescaled results for J_z^+ and J_z^- are shown in Fig. S3 of the Supplementary Material. These were found in the vapour at the distance $z = 15$ to be $J_z^+ = 2.0$ and $J_z^- = 0.07$, i.e. 3.5 % of the evaporated particles were backscattered, which is the same result as in the low temperature case. From the particle flux j_z^E of Runs 4 and 5, the evaporation coefficient $\alpha = 0.865$ can be calculated.

At $T_1 = 0.85$ the NEMD values for the vapour deviate much stronger from the Hertz assumption, where in particular the evaporation coefficient $\alpha = 0.86$ is definitely lower than

unity. The decrease of α cannot be explained by the backflux, because it amounts only 3.5 %, which would raise α to about 0.90. A potential explanation for the deviations between the NEMD data from Hertz theory can be based on the energy required for evaporation, which is supplied as heat and henceforth called heat of evaporation. Hertz made his assumptions for low temperatures and thus low vapour pressures, which means small particle fluxes. For that case he could implicitly assume that the heat of evaporation is supplied from the bulk of the liquid without significant changes of its properties up to the surface. This assumption is justified as long as the particle flux is small, which was in essence confirmed by the present study for low temperature evaporation. At the medium temperature, however, where the particle flux is larger, more energy has to be transported to the surface to supply the required heat of evaporation. This can be done according to Fourier's law for heat conduction $q_z = -\lambda_H \, dT/dz$ (with λ_H being the thermal conductivity) by a decrease of the temperature approaching the interface. This implies that the particles evaporate from an interface with a temperature which is lower than the bulk liquid temperature T_1 and hence the original assumptions of Hertz do not hold any more. This trend should become more apparent for higher temperatures as discussed below.

Moreover, Fig. 7 shows contracted velocity distribution functions $\hat{f}_z$ in the liquid and the vapour sampled either directly from the NEMD simulations or obtained as Maxwellians according to Eq. (7) with temperatures and drift velocities in the liquid and the vapour from Table 1. In the liquid, the directly sampled values match very well with the Maxwellian. In the vapour, some scattering of the directly sampled values with a shift of the maximum to lower velocities than in the Maxwellian was observed.

4.3. Evaporation at high temperature

The high temperature T_1 = 1.10 is equivalent to T_1/T_c= 0.840. For methane at 0.840T_c = 160.07 K, the vapour pressure is 16.0 bar, which is a rather high evaporation pressure.

At T_1 = 1.10, Runs 7 and 8 were carried out with L_z = 48.3 and Run 9 with L_z = 81.6. Hence, the length of the vapour phase was L_v = 14 for Runs 7 and 8, whereas L_v = 31 for Run 9, cf. Table 1. The mean free path λ in the vapour varied from 11.5 for Runs 7 and 8 to 15 for Run 9, which means that Kn = λ/L_v = 0.82 for Runs 7 and 8 and Kn = 0.49 for Run 9. In other words, in Runs 7 and 8 each particle underwent on average one collision in the vapour phase, while in Run 9 two collisions occured on average. The number of sampled NEMD time steps M was 50,000 for Runs 7 and 8 and 30,000 for Run 9. Longer runs were not thought to be necessary because of the comparatively high vapour density.

Profiles for the density $\rho(z)$, the temperatures $T_{xy}(z)$ and $T_z(z)$ and for the drift velocity $v_z^D(z)$ from Run 9 are shown in Fig. 8. The corresponding profiles from Run 7 are given in Fig. S4 of the Supplementary Material. For the vapour it is known from kinetic theory [8] that due to collisions 1) the temperature and the density vary over distance z for a given vapour volume length L_v and 2) the flow pattern changes with increasing length L_v.

From Fig. 8 in combination with Table 1, it can be noted that the density $\rho(z)$ in case of evaporation starts in the liquid from a 2% lower value than the saturated liquid density ρ', but then increases to a maximum which is 2% higher than ρ'. The same effect was also found in Refs. [19-22] at the corresponding temperatures and it might be caused by the recoil of the strong evaporation flux. The density in the vapour ρ_{ve} decreases to 37% of the saturated vapour density ρ'' for Runs 7 and 8 and to 28% for Run 9. For the latter, the interfacial width

was found to be w = 3.1. Except for the small maximum on the liquid side and the decrease of the vapour density ρ_{ve}, the density profile $\rho(z)$ did not change much in the interface even during strong evaporation as can be seen from Fig. 9, where the density profiles for equilibrium conditions and steady state evaporation into vacuum are compared.

The temperature profiles T_{xy} and T_z shown in Fig. 8 start to decrease already in the liquid. The temperature T_{xy} shows a tendency towards a linear decrease, whereas for T_z the steepest slope starts at the end of the interface. The decrease of the temperatures in the liquid and in the interface can again be explained by the heat transport required for supplying the heat of evaporation. The further decrease of the temperature in the vapour is in agreement with kinetic theory [8] and is thought to be coupled to the increase of the drift velocity $v_{z,ve}^D$ with increasing z. For Run 9 the "bulk" drift velocity is $v_{z,ve}^D$ = 0.84 and raises up to $v_{z,ve,\max}^D$ = 0.96, cf. Fig. 8. Hence, the ratio of the maximum drift velocity to the sound velocity was $v_{z,ve,\max}^D / c$ = 0.91.

Considering the results for the particle fluxes j_z^E and j_z^D from the Runs 7 to 9 given in Table 1, it can be seen that they agree well with each other. Taking the average value j_z^E = 0.0125 of the shorter Runs 7 and 8 and the Hertz flux j_z^{+H} = 0.02251, an evaporation coefficient α = 0.555 was obtained. In Run 9, the particle flux j_z^D was separated into j_z^+ and j_z^- and the rescaled fluxes J_z^+ and J_z^- are shown in Fig. 10. It was found that the backflux j_z^- amounts 5.2% of j_z^D, which would raise the evaporation coefficient α from 0.555 to 0.583.

The kinetic heat flux in the liquid for the high temperature was calculated according to Eq. (27). This calculation is not very accurate, because it requires third moments for which the

NEMD simulations gave $\left\langle v_x^2 v_z \right\rangle$ = 0.0384, $\left\langle v_y^2 v_z \right\rangle$ = 0.0373 and $\left\langle v_z^3 \right\rangle$ = 0.106. Therefrom, the kinetic heat flux was obtained as q = 0.043. On the other hand, if the heat flux q_e is calculated on the basis of the enthalpy of evaporation Δh_v = 4.7 [35] and the particle flux j_z^E = 0.0125 according to

$$q_e = j_z \Delta h_v, \tag{30}$$

q_e = 0.059 is obtained. Hence, the heat flux q is 27% lower than the heat flux q_e, which is a reasonable agreement in view of the simulation uncertainties.

Finally, contracted velocity distribution functions $\hat{f}_z$ in the liquid and the vapour are shown in Fig. 11. Here, even in the vapour only a small scatter of the directly sampled values around the Maxwellian distribution was observed.

5. Evaporation coefficient

A compilation of simulation based evaporation coefficients α as a function of the reduced temperature T_l/T_c was given by Xie et al. in Fig. 10 of Ref. [13]. Results are shown for argon, methanol, water and n-dodecane from different authors who used different methodologies. These results differ at a given reduced temperature T/T_c by up to 100%. The conclusion in Ref. [13] is that "in all cases the condensation coefficient decreases when the liquid temperature increases". A detailed discussion of these results, however, was not given there. We believe that the evaporation coefficient α depends like the thermodynamic equilibrium and transport properties on the intermolecular and also to some extent on the intramolecular interactions. This view is supported by some impressions from Fig. 10 of Xie et al. [13]: i) The results for n-dodecane are close to those of argon, ii) the results for methanol are the lowest. Hence, one may raise the hypotheses that inelastic collisions play a minor role and the

dipole moment plays a larger role for the evaporation coefficient. The latter effect may be caused by the orientational behaviour of the dipolar molecules found in the liquid-vapour interface [58, 59].

Our aim was to work out the temperature dependence of the evaporation coefficient α in more detail. For that purpose, we compare the results for LJ type fluids from this work, from Anisimov et al. [19], from Ishiyama et al. [20] and from Tsuruta et al. [15] in Fig. 12, which shows α as function of T/T_c. Whilst in the first three sources NEMD simulations were made for evaporation into vacuum, Tsuruta et al. determined α via equilibrium simulations.

We defined α in Eq. (29) by $\alpha = j_z^E / j_z^{+H}$ and presented the results for the full LJ fluid in Table 1. It can be seen that the results from different NEMD runs for the same thermostat temperature T_1 differ slightly. Hence, we determined average values and statistical uncertainties Δ_{runs}, being $\Delta_{runs} = 0.005$ for $T_1 = 0.70$ ($T_1/T_c = 0.534$), $\Delta_{runs} = 0.005$ for $T_1 = 0.85$ ($T_1/T_c = 0.649$) and $\Delta_{runs} = 0.025$ for $T_1 = 1.10$ ($T_1/T_c = 0.840$). Moreover, it was estimated above that the maximum upward correction due to the backflux is 3.5% for the two lower temperatures and 5.2% for $T_1 = 1.10$. Hence, the values for the evaporation coefficient (with upper and lower error limits given in brackets) are $\alpha = 1.005$ (1.00, 1.04) at $T_1 = T_1/T_c = 0.534$, $\alpha = 0.865$ (0.86, 0.90) at $T_1/T_c = 0.649$ and $\alpha = 0.555$ (0.53, 0.61) at $T_1/T_c = 0.840$.

Anisimov et al. [19] considered the LJ3.5 fluid and found for the critical temperature $T_{cLJ3.5} = 1.21$. It can be seen from Fig. 12 that their results match reasonably well with the present data for high temperatures. This agreement, however, becomes worse with decreasing temperature. In the temperature range T/T_c between 0.615 and 0.695, the α values of Anisimov et al. [19] scatter around $\alpha = 0.75$, whereas we obtained $\alpha = 0.86$ at $T/T_c = 0.649$.

As the saturated vapour density ρ'' enters directly into the Hertz flux j_z^{+H}, we have compared the $\rho''_{LJ3.5}$ results from Ref. [19] with the ρ''_{LJ} values from the correlation equation for the LJ fluid [35]. For the six temperatures k_BT/ε = 0.752, 0.891, 0.842, 0.900, 0.900 and 1.00 we found for the deviations ($\rho''_{LJ3.5}/\rho''_{LJ}$ - 1) the following values: 0.69, 0.57, 0.62, 0.49, 0.33 and 0.46. Of course, the saturated vapour densities of the LJ3.5 fluid have to be higher than those of the LJ fluid according to the explanations in Sec. 1, but this sequence of deviations indicates a strong scatter of the saturated vapour densities which propagates into the evaporation coefficient α.

Ishiyama et al. [20] considered the LJ4.4 fluid in the temperature range T/T_c between 0.568 and 0.897. From Fig. 12, it can be seen that their results lie on a smooth curve and are 10% lower at our highest temperature and 13% lower than ours at their lowest temperature. A comparison of their saturated vapour densities at the six temperatures k_BT/ε = 0.7095, 0.7513, 0.8347, 0.9182, 1.0017 and 1.0851 with the ρ''_{LJ} values from the correlation equation for the LJ fluid [35] gives deviations ($\rho''_{LJ4.4}/\rho''_{LJ}$ - 1) of 0.25, 0.26, 0.21, 0.24, 0.22 and 0.22. This comparison is satisfying as the increase of ρ'' had to be expected and the scattering of the deviation is very small over that large temperature range. The remaining question is about the differences in α of 10 % to 13 % between the Ishiyama et al. results and ours. Of course, these could be due to simulation uncertainties, but because these deviations are systematic this explanation is less likely. A possible explanation could be that the potential cut-off has a stronger effect on increasing the saturated vapour density than on increasing the evaporation flux.

In the work of Tsuruta et al. [15], test particles were injected from the vapour side onto the interface region under equilibrium for an LJ3.5 fluid. This method does not depend so much

on the saturated vapour density but rather on the statistics of particle trajectories. The results shown in Fig. 12 were obtained from Eq. (2) in combination with Table 1 of Ref. [15]. In order to obtain the reduced temperature we adopted ε/k_B = 119.8 K from Ref. [15] and assumed the critical temperature of the LJ3.5 fluid to be $T_{cLJ3.5}$ = 1.21 according to Anisimov et al. [19]. Ignoring the outlying data point at T/T_c = 0.62 (T = 90 K), there is a surprisingly good agreement with the present results. At the lowest temperature T/T_c = 0.58 (T = 84 K) the deviation is only $(\alpha_{Tsuruta}/\alpha_{Lotfi}$ -1) = -0.06, whilst at the highest temperature T/T_c = 0.90 (T = 130 K) the deviation is +0.11.

For practical applications, it would be helpful to have a method for estimating the evaporation coefficient. Anisimov et al. [19] obtained a value of $\alpha \approx 0.80$ in case that j_z^{+H} was calculated for the temperature T_{Kn} of the dividing surface where the evaporation begins, i.e. where the drift velocity $v_{z,ve}^D$ becomes nonzero and where the kinetic temperatures $T_{xy,ve}$ and $T_{z,ve}$ start to diverge. The practical problem then is to determine T_{Kn}. In our understanding T_{Kn} can only be determined if the temperature and the density profile are known over the whole range of the interface, which seems to be equally or even more complicated than to determine α directly. Hołyst and Litniewski [21] suggested the calculation of the particle flux via the pseudo-temperature T_{out}, which is determined from the average kinetic energy in the vapour flux. To our opinion, this is also not a very practical method, because T_{out} has to be measured [21].

Instead, we suggest a simple correlation for the evaporation coefficient α as a function of the reduced temperature T/T_c, which is based on the present NEMD results. As we have shown that for the low temperature T/T_c = 0.534, the assumptions of Hertz for the vapour density ρ, the total kinetic temperature T and the particle flux j are confirmed by NEMD

simulations, we specify for the lower temperature range $\alpha = 1$. For higher temperatures we assume a straight line $\alpha = a + b(T/T_c)$ based on $\alpha = 0.865$ at $T/T_c = 0.649$ and $\alpha = 0.555$ at $T/T_c = 0.840$. The transition from the lower to the higher temperature range should occur at the intersection point of the two straight lines. Hence we obtain the correlation

$$\alpha = 1, \qquad \text{for } T/T_c \le 0.5659, \tag{31a}$$

$$\alpha = 1.9184 - 1.6230\ (T/T_c), \qquad \text{for } T/T_c \ge 0.5659, \tag{31b}$$

which is shown in Fig. 12.

6. Summary and Conclusions

The present paper describes an investigation of steady state evaporation from a planar liquid surface into vacuum by non-equilibrium molecular dynamics simulations of a fluid with full LJ interactions. Studies were made for the reduced liquid temperatures $T/T_c = 0.53$, 0.65 and 0.84. The reduced temperature $T/T_{cLJ} = 0.53$ corresponds to a vapour pressure of 0.41 bar for methane and is the lowest temperature that was studied for a LJ type fluid so far. Results were given for the profiles of the density $\rho(z)$, the kinetic temperature $T(z)$ and its components $T_{xy}(z)$ and $T_z(z)$, the drift velocity $v_z^D(z)$ as well as for the total particle flux j_z calculated in two different ways. Further, the outgoing and incoming particle fluxes were separated, at the high temperature the kinetic heat flux was calculated, and comparisons with kinetic theory were made. Moreover, velocity distribution functions were shown. From the total particle flux j_z, the evaporation coefficient α was calculated and its statistical uncertainty estimated.

It was found for all temperatures that the density profile does not change significantly in the liquid and in the interface in comparison with that under equilibrium conditions.

At the low temperature, the vapour density, the vapour temperature and the particle flux obtained from the NEMD simulations agree very well with the values obtained from the assumption of Hertz that the outgoing velocity distribution function is a half-sided Maxwellian with the bulk liquid temperature T_1 and the saturated vapour density ρ''. This implies that the evaporation coefficient $\alpha = 1$ was confirmed. Only the kinetic temperature components T_{xy} and T_z showed a tendency to reduce their difference compared to the Hertz values.

For the medium and high temperatures, the kinetic temperatures decrease slightly already in the liquid and stronger in the interface, which causes a lower particle flux than assumed by Hertz and hence α decreases with the temperature. Our hypothesis is that the Hertz assumption does not take into account the larger flux of heat of evaporation, which is required for the higher particle fluxes at higher temperatures. According to Fourier's law for heat conduction, however, more heat can be transported to the surface by a decrease of the temperature in approaching the surface. This implies that the particles evaporate from an interface with a lower temperature than the bulk liquid temperature. It is conjectured that a deeper understanding of this behaviour can be obtained by using a kinetic theory of fluids based on the Bogoliubov–Born–Green–Kirkwood–Yvon hierarchy as outlined in Ref. [17] or by using non-equilibrium density functional theory [57].

Finally, a simple correlation was given to estimate α as a function of the reduced temperature T/T_c. One should be aware that this correlation was derived for the fluid with full LJ interactions which is generally considered as a reference fluid. According to the discussion in Sec. 5 we expect, however, modifications of this correlation for other intermolecular

interactions. A systematic investigation of these modifications remains a challenging task for the future.

Acknowledgements

The authors thank Professor Takaharu Tsuruta from Kyushu Instititute of Technology, Japan, for provision of literature and Dr. Dietmar Möller from Merck KGaA, Darmstadt, Germany. for fruitful discussions. They gratefully acknowledge funding of this work by Deutsche Forschungsgemeinschaft (DFG) under grant numbers Fi 287/6 and Vr 6/9.

References

[1] H. Hertz, I. Über die Verdunstung der Flüssigkeiten, insbesondere des Quecksilbers, im luftleeren Raume, Ann. Phys. 253 (1882) 177-193.

[2] M. Knudsen, Die maximale Verdampfungsgeschwindigkeit des Quecksilbers, Ann. Phys. 352 (1915) 697-708.

[3] M. Volmer, Kinetik der Phasenbildung, Steinkopff-Verlag, Dresden, Leipzig, 1939.

[4] P. Welander, On the temperature jump in a rarefied gas, Ark. Fys. 7 (1954) 507-533.

[5] P.L. Bhatnagar, E.P. Gross, K. Krook, A model for collision processes in gases, Phys. Rev. 94 (1954) 511-524.

[6] M.N. Kogan, Rarefied Gas Dynamics, Plenum Press, New York, 1969.

[7] S.I. Anisimov, A.Kh. Rakhmatulina, The dynamics of the expansion of a vapor when evaporated into a vacuum, Zh. Eksp. Teor. Fiz. 64 (1973) 869-876 [Sov. Phys. JETP 37 (1973) 441-444].

[8] J. Fischer, Distribution of pure vapour between two parallel plates under the influence of strong evaporation and condensation, Phys. Fluids 19 (1976) 1305-1311.

[9] S.S. Sazhin, I.N. Shishkova, A.P. Kryukov, V.Yu. Levashov, M.R. Heikal, Evaporation of droplets into a background gas: Kinetic modelling, Int. J. Heat Mass Transfer 50 (2007) 2675-2691.

[10] A. Lotfi, J. Fischer, MD simulation results on the dynamics in the liquid-vapour interface, Ber. Bunsenges. Phys. Chemie 94 (1990) 294-297.

[11] K. Yasuoka, M. Matsumoto, Y. Kataoka, Evaporation and condensation at a liquid surface. I. Argon, J. Chem. Phys. 101 (1994) 7904-7911.

[12] M. Matsumoto, K. Yasuoka, Y. Kataoka, Evaporation and condensation at a liquid surface. II. Methanol, J. Chem. Phys. 101 (1994) 7912-7917.

753 [13] J.-F. Xie, S. S. Sazhin, B.-Y. Cao, Molecular dynamics study of the processes in the
754 vicinity of the n-dodecane vapour/liquid interface, Phys. Fluids 23 (2011) 112104.
755 [14] T. Tsuruta, N. Sakamoto, T. Masuoka, Condensation process at liquid-vapor interface
756 and condensation coefficient, Thermal. Sci. Eng. 3 (1995) 85-90.
757 [15] T. Tsuruta, H. Tanaka, T. Masuoka, Condensation/Evaporation coefficient and
758 velocity distributions at liquid-vapor interface, Int. J. Heat Mass Transfer 42 (1999)
759 4107-4116.
760 [16] G. Nagayama, T. Tsuruta, A general expression for the condensation coefficient based
761 on transition state theory and molecular dynamics simulation, J. Chem. Phys. 118
762 (2003) 1392-1399.
763 [17] A. Lotfi, Molekulardynamische Simulationen an Fluiden: Phasengleichgewicht und
764 Verdampfung, PhD thesis, Ruhr-Universität-Bochum, Germany, 1993.
765 [18] V.V. Zhakhovskii, S.I. Anisimov, Molecular-dynamics simulation of evaporation of a
766 liquid, Zh. Eksp. Teor. Fiz. 111 (1997) 1328-1346 [Sov. Phys. JETP 84 (1997) 734-
767 745].
768 [19] S.I. Anisimov, D.O. Dunikov, V.V. Zhakhovskii, S.P. Malyshenko, Properties of a
769 liquid-gas interface at high-rate evaporation, J. Chem. Phys. 110 (1999) 8722-8729.
770 [20] T. Ishiyama, T. Yano, S. Fujikawa, Molecular dynamics study of kinetic boundary
771 condition at an interface between argon vapour and its condensed phase. Phys. Fluids
772 16 (2004) 2899-2906.
773 [21] R. Hołyst, M. Litniewski, Evaporation into vacuum: Mass flux from momentum flux
774 and the Hertz-Knudsen relation revisited, J. Chem. Phys. 130 (2009) 074707(1-6).
775 [22] S. Cheng, J.B. Lechman, S.J. Plimpton, G.S. Grest, Evaporation of Lennard-Jones
776 Fluids, J. Chem. Phys. 134 (2011) 22704(1-13).

777 [23] J. Yu, H. Wang, A molecular dynamics investigation on evaporation of thin liquid
778 films, Int. J. Heat Mass Transfer 55 (2012) 1218-1225.
779 [24] N.L. Long, M.M. Micci, and B.C. Wong, Molecular dynamics simulation of droplet
780 evaporation, Comput. Phys. Commn. 96 (1996) 167-172.
781 [25] M.M. Micci, T.L. Kaltz, L.N. Long, Molecular dynamics simulations of micrometer-
782 scale droplet vaporization, Atomization and Sprays 11 (2001) 653- 666.
783 [26] L. Consolini, S.K. Aggarwal, S. Murad, A molecular dynamics simulation of droplet
784 evaporation, Int. J. Heat Mass Transfer 46 (2003) 3179-3188.
785 [27] S. Sumardiono, J. Fischer, Molecular simulations of droplet evaporation processes:
786 Adiabatic pressure jump evaporation, Int. J. Heat Mass Transfer 49 (2006) 1148-1161.
787 [28] S. Sumardiono, J. Fischer, Molecular dynamics simulations of mixture droplet
788 evaporation, In: J. Pagliarini / S. Rainieri (Eds.): Proc. Eurotherm Seminar 77, Heat
789 and Mass Transfer in Food Processing, 20.06.2005 - 22.06.2005, Parma, 323-328;
790 Edizione ETS Parma, Parma; ISBN 88-467-1302-8.
791 [29] S. Sumardiono, J. Fischer, Molecular simulations of droplet evaporation by heat
792 transfer, Microfluidics and Nanofluidics 3 (2007) 127-140.
793 [30] E. Landry, S. Mikkilineni, M. Paharia, A. McGaughey, Droplet evaporation: A
794 molecular dynamics investigation, J. Appl. Phys. 102 (2007) 124301(1-7).
795 [31] R. Hołyst, M. Litniewski, Heat transfer at the nanoscale: Evaporation of nanodroplets,
796 Phys. Rev. Lett. 100 (2008) 055701(1-4).
797 [32] J. Zhang, F. Müller-Plathe, M. Yahia-Ouahmed, F. Leroy, A steady-state non-
798 equilibrium molecular dynamics approach for the study of evaporation processes, J.
799 Chem . Phys. 139 (2013) 134701.

800 [33] K. Bucior, L. Yelash, K. Binder, Molecular dynamics simulation of evaporation
801 processes of fluid bridges confined in slit-like pore, Phys. Rev. E 79 (2009) 031604(1-
802 12).
803 [34] A. Lotfi, J. Vrabec, J. Fischer, Orthobaric densities from simulations of the liquid
804 vapour interface, Mol. Simul. 5 (1990) 233-243.
805 [35] A. Lotfi, J. Vrabec, J. Fischer, Vapour liquid equilibria of the Lennard-Jones fluid
806 from the *NpT* + test particle method, Mol. Phys. 76 (1992) 1319-1333.
807 [36] J. Kolafa, I. Nezbeda, The Lennard-Jones fluid: An accurate analytic and theoretically-
808 based equation of state, Fluid Phase Equilib. 100 (1994) l-34.
809 [37] M. Mecke, A. Müller, J. Winkelmann, J. Vrabec, J. Fischer, R. Span, W. Wagner,
810 An accurate van der Waals type equation of state for the Lennard-Jones fluid, Int. J.
811 Thermophysics 17 (1996) 391-404 and 19 (1998) 1493-1493.
812 [38] J.K. Johnson, J.A. Zollweg, K.E. Gubbins, The Lennard-Jones equation of state
813 revisited, Mol. Phys. 78 (1993) 591-618.
814 [39] M. Mecke, J. Winkelmann, J. Fischer, Molecular dynamics simulation of the liquid-
815 vapor interface: The Lennard-Jones fluid, J. Chem. Phys. 107 (1997) 9264-9270.
816 [40] A. Ahmed, R.J. Sadus, Solid-liquid equilibria and triple points of *n*-6 Lennard-Jones
817 fluids, J. Chem. Phys. 131 (2009) 174504.
818 [41] E. A. Mastny, J.J. de Pablo, Melting line of the Lennard-Jones system, infinite size,
819 and full potential, J. Chem. Phys. 127 (2007) 104504.
820 [42] W. van Megen, I.K. Snook, Physical adsorption of gases at high pressure I. The critical
821 region. Molec. Phys. 45 (1982) 629.
822 [43] B. Smit, Phase diagrams of Lennard-Jones fluids, J. Chem. Phys. 96 (1992) 8639-
823 8640.

824 [44] J. Vrabec, G.K. Kedia, G. Fuchs, H. Hasse, Comprehensive study of the vapour-liquid
825 coexistence of the truncated and shifted Lennard-Jones fluid including planar and
826 spherical interface properties, Mol. Phys. 104 (2006) 1509-1527.
827 [45] A. Z. Panagiotopoulos, Molecular simulation of phase coexistence: Finite-size effects
828 and determination of critical parameters for two- and three-dimensional Lennard-Jones
829 fluids, Int. J.Thermophysics 15 (1994) 1057-1072
830 [46] J. Vrabec, J. Stoll, H. Hasse, A set of molecular models for symmetric quadrupolar
831 fluids, J. Phys. Chem. B 105 (2001) 12126-12133.
832 [47] R.W. Schrage, A Theoretical Study of Interface Mass Transfer, Columbia University
833 Press, New York, 1953.
834 [48] H.K. Cammenga, Evaporation mechanisms of liquids, in Current Topics in Materials
835 Science, Vol. V/4, E. Kaldis (Ed.), North-Holland Publishing Company, Amsterdam,
836 1980, pp. 335-446.
837 [49] I. W. Eames, N. J. Marr, H. Sabir, The evaporation coefficient of water: a review. Int.
838 J. Heat Mass Transfer 40 (1997) 2963-2973.
839 [50] R. Marek, J. Straub, Analysis of the evaporation coefficient and the condensation
840 coefficient of water. Int. J. Heat Mass Transfer 44 (2001) 39-53.
841 [51] C. A. Ward, D. Stanga, Interfacial conditions during evaporation or condensation of
842 water, Phys. Rev. E 64 (2001) 051509.
843 [52] O.E. Shklyaev, E. Fried, Stability of an evaporating thin liquid film, J. Fluid Mech.
844 584 (2007) 157-183.
845 [53] C.W. Gear, Numerical Initial Value Problems in Ordinary Differential Equations,
846 Prentice Hall, Englewood Cliffs, 1971.
847 [54] J.M. Haile, Molecular Dynamics, Elementary Methods, Wiley, New York, 1992. C

[55] I. Nezbeda, J. Kolafa, A new version of the insertion particle method for the determining the chemical potential by Monte Carlo simulation, Mol. Simul. 5 (1991) 391-403.hia

[56] U. Setzmann, W. Wagner, A new equation of state and tables of thermodynamic properties for methane covering the range from the melting line to 625 K at pressures up to 1000 MPa**,** J. Phys. Chem. Ref. Data 20 (1991) 1061-1151.),

[57] E. Johannessen, J. Gross, D. Bedeaux, Nonequilibrium thermodynamics of interfaces using classical density functional theory, J. Chem. Phys. 129 (2008) 184703(1-14).

[58] M. Mecke, J. Fischer, und J. Winkelmann, Molecular dynamics simulation of the liquid-vapor interface of dipolar fluids under different electrostatic boundary conditions. J.Chem. Phys.114 (2001) 5842 – 5852.

[59] S. Enders, H. Kahl, M. Mecke, J. Winkelmann, Molecular dynamics simulation of the liquid–vapor interface: I. The orientational profile of 2-center Lennard–Jones and of Stockmayer fluid molecules. J. Molec.Liquids 115 (2004) 29–39.

Figures

Fig. 1.

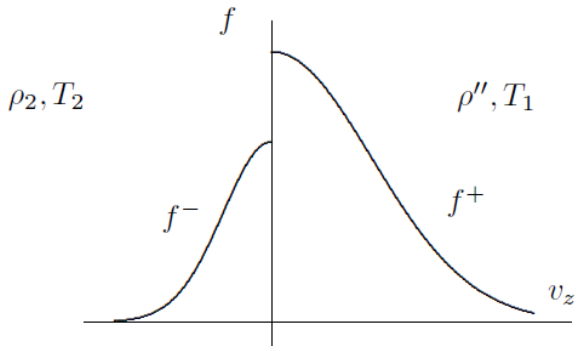

Fig 1.: Contracted half-sided Maxwellian distribution functions which are usually assumed in kinetic theory as boundary conditions for evaporation from a planar liquid surface.

Fig. 2.

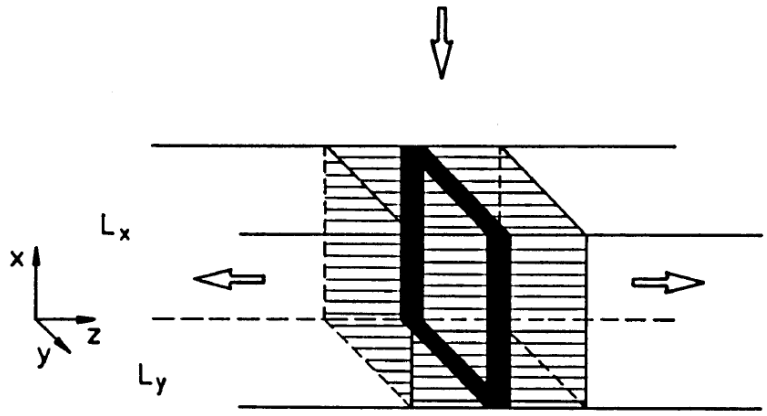

Fig 2.: Schematic representation of the simulation volume with the liquid slab in the middle (hatched). In the volume with a width of 4σ in the centre of the liquid marked in black, the temperature T_1 was kept constant by momentum scaling. The horizontal arrows represent the evaporated particles which were removed if they crossed the virtual planes on the left or the right side and were reinserted in the centre of the liquid, as indicated by the vertical arrow.

Fig. 3.

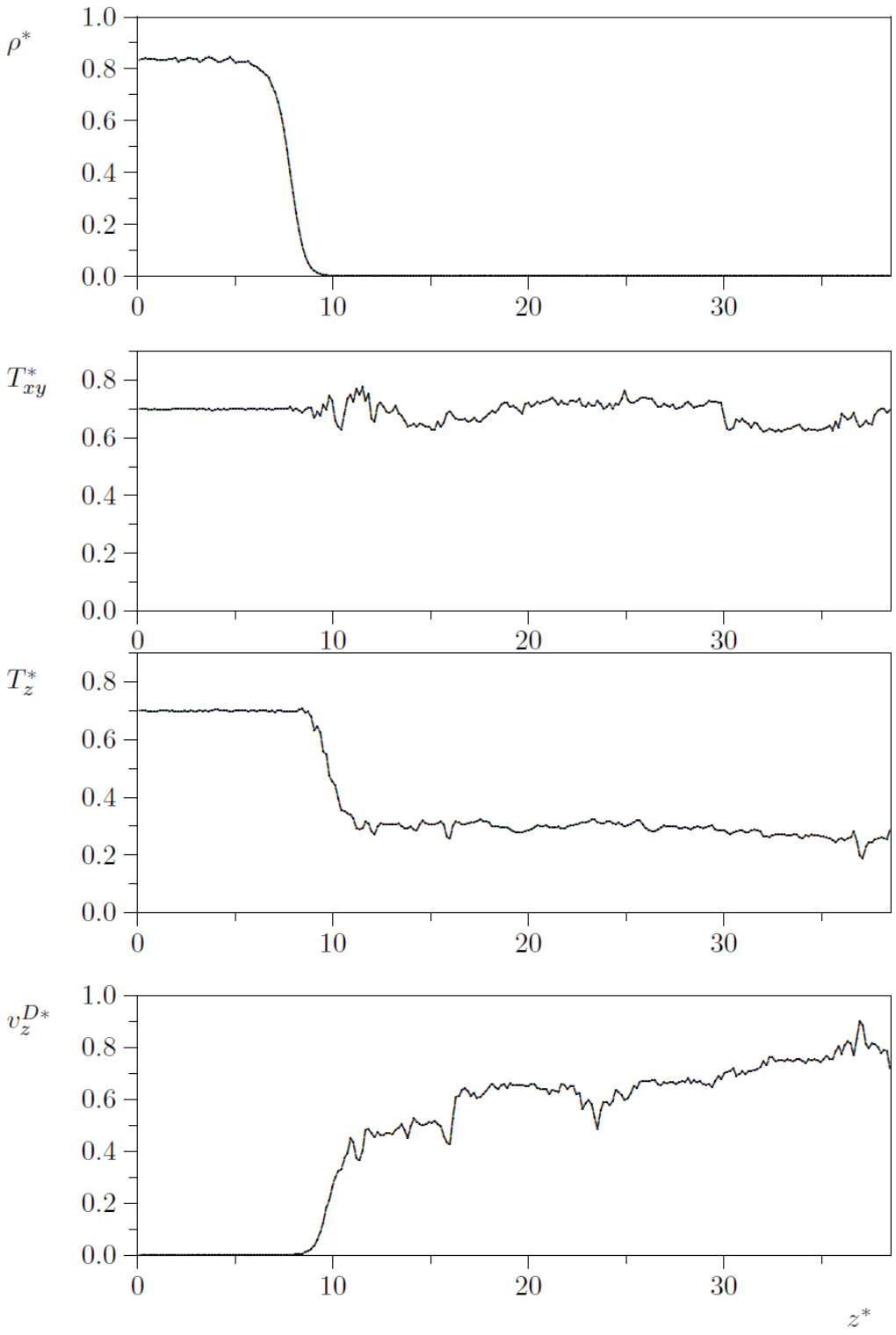

Fig. 3.: Evaporation into vacuum at T_1 = 0.70. NEMD profiles for the density ρ, the temperature components T_{xy} and T_z and the drift velocity v_z^D up to $z = L_z/2$ from Run 3.

Fig. 4.

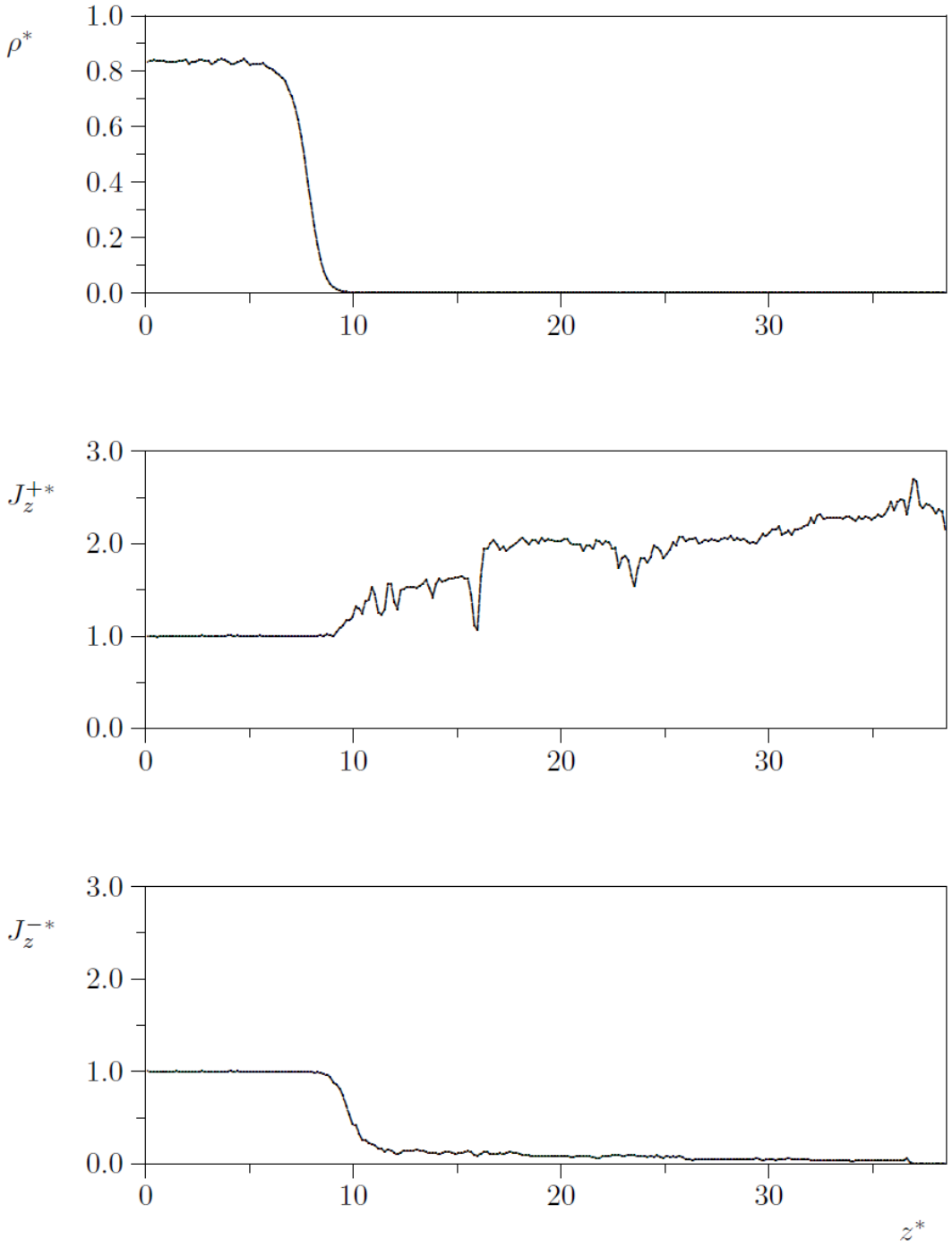

Fig. 4.: Evaporation into vacuum at T_1 = 0.70. NEMD profiles for the density ρ as well as for the scaled outgoing and incoming particle fluxes J_z^+ and J_z^- from Run 3. The scaling was made with respect to the Hertz flux at the local density $\rho(z)$ and the temperature T_1 according to $J_z^+ = j_z^+/[\rho(z)(T_1/2\pi)]$.

Fig. 5.

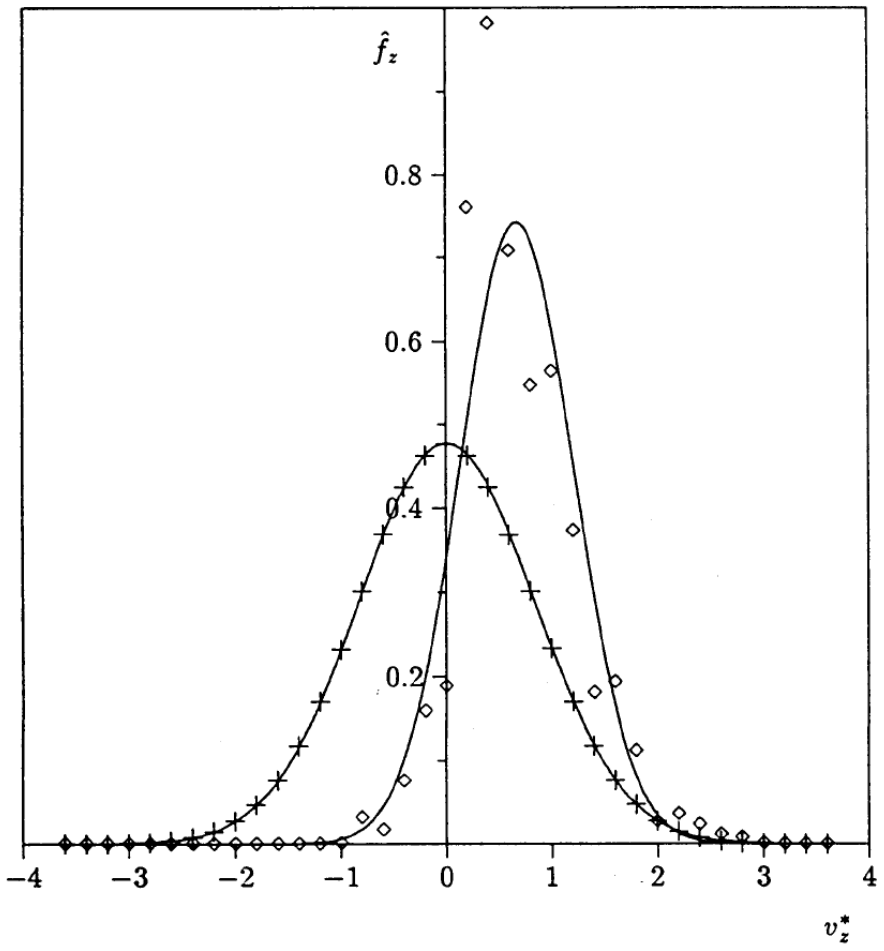

Fig. 5.: Contracted velocity distribution functions $\hat{f}_z$ for evaporation into vacuum at $T_1 = 0.70$. The crosses + denote data that were directly sampled by NEMD in the liquid, the diamonds ◊ denote data that were directly sampled in the vapour. The solid curves are Maxwellians according to Eq. (7) with temperatures and drift velocities for the liquid and the vapour as given in Table 1.

915 Fig. 6.

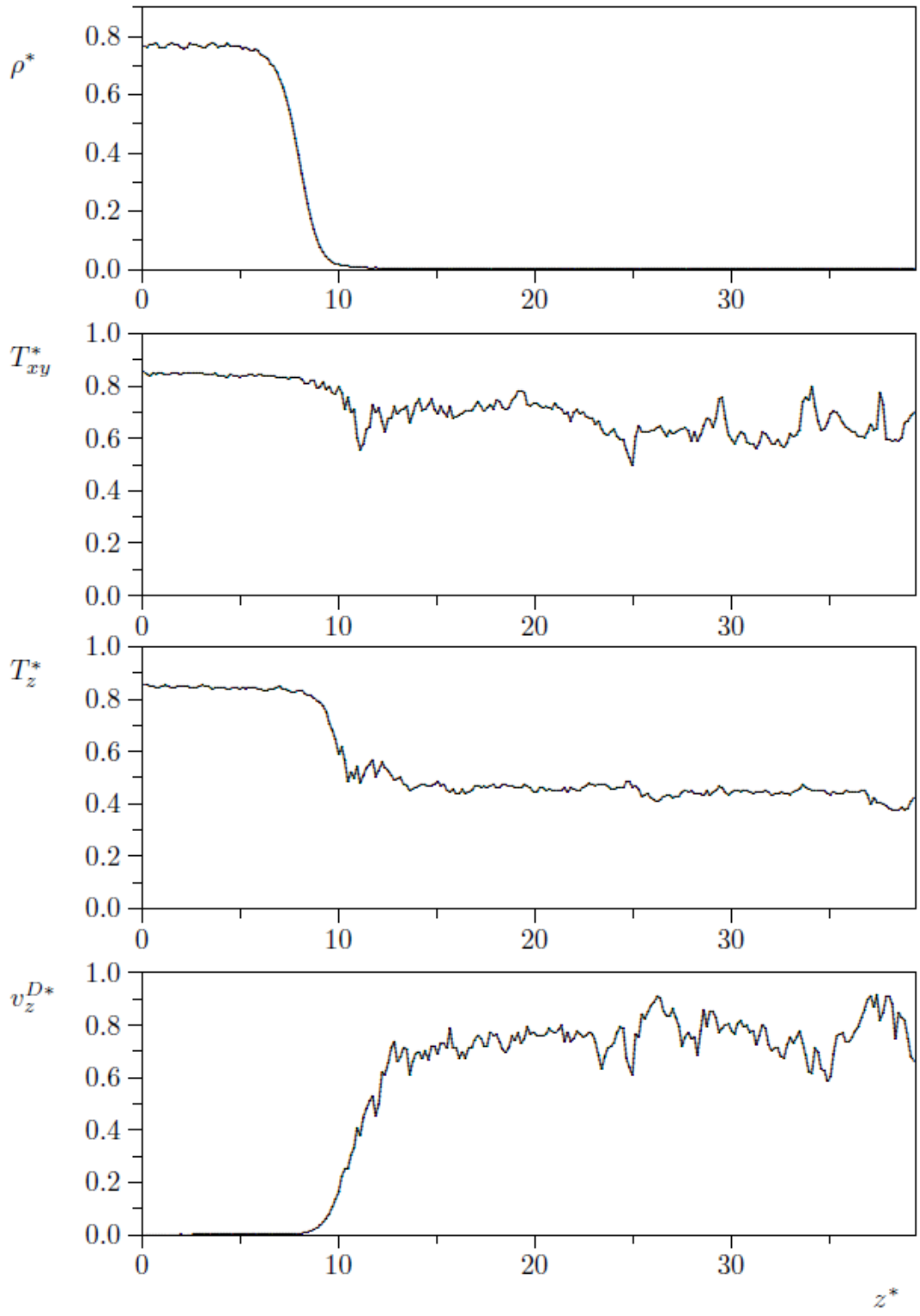

916

917 Fig 6: Evaporation into vacuum at T_1 = 0.85. NEMD profiles for the density ρ, the

918 temperature components T_{xy} and T_z and the drift velocity v_z^D up to $z = L_z/2$ from Run 6.

Fig. 7.

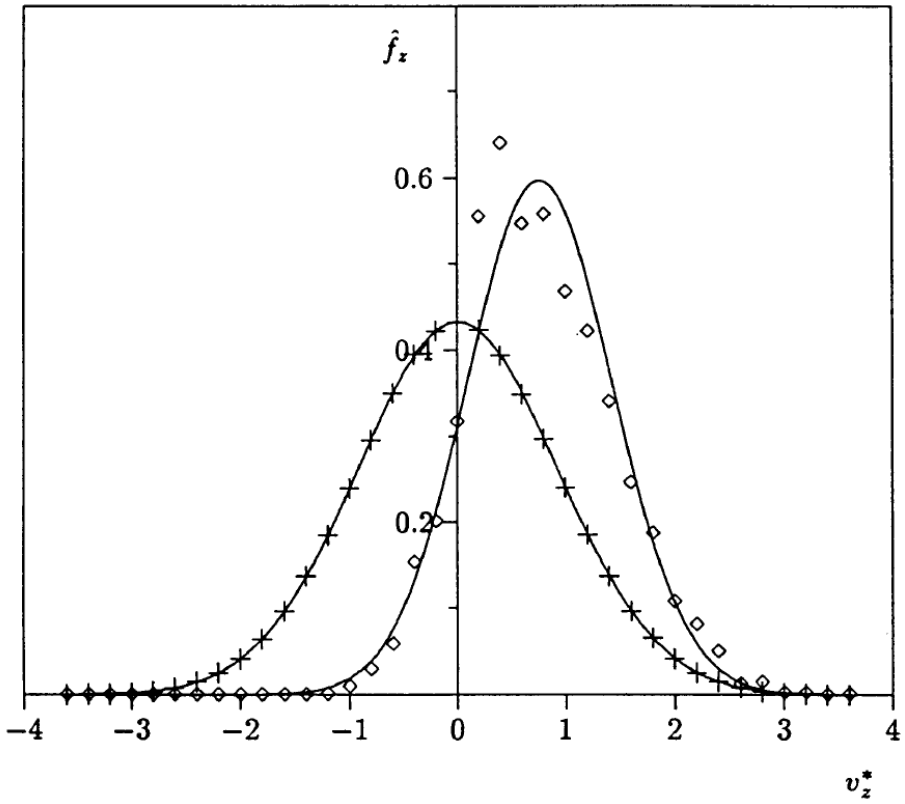

Fig. 7.: Contracted velocity distribution functions $\hat{f}_z$ for evaporation into vacuum at $T_1 = 0.85$. The crosses + denote data that were directly sampled by NEMD in the liquid, the diamonds ◊ denote data that were directly sampled in the vapour. The solid curves are Maxwellians according to Eq. (7) with temperatures and drift velocities for the liquid and the vapour as given in Table 1.

Fig. 8.

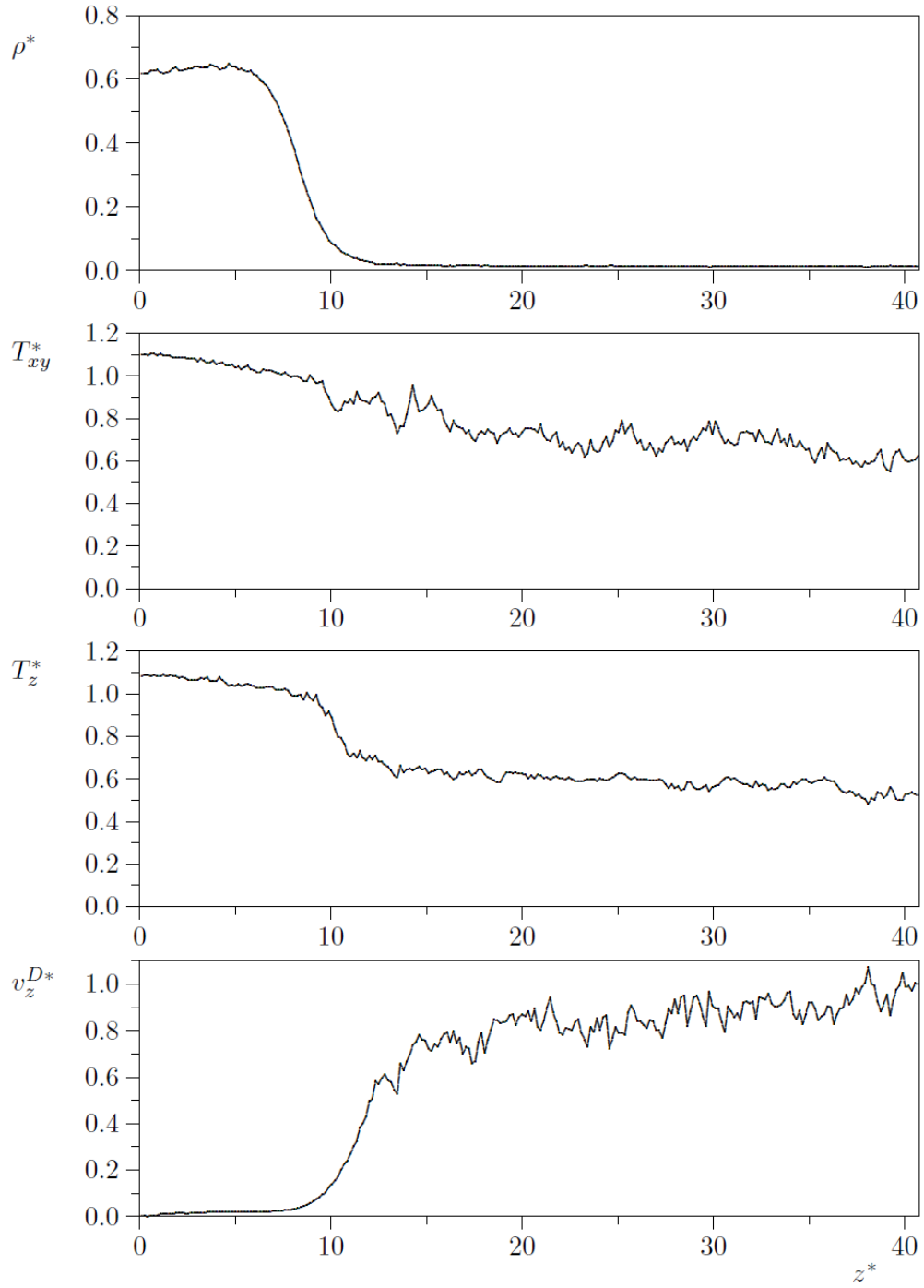

Fig 8: Evaporation into vacuum at T_1 = 1.10. NEMD profiles for the density ρ, the temperature components T_{xy} and T_z and the drift velocity v_z^D up to $z = L_z/2$ from Run 9.

Fig. 9.

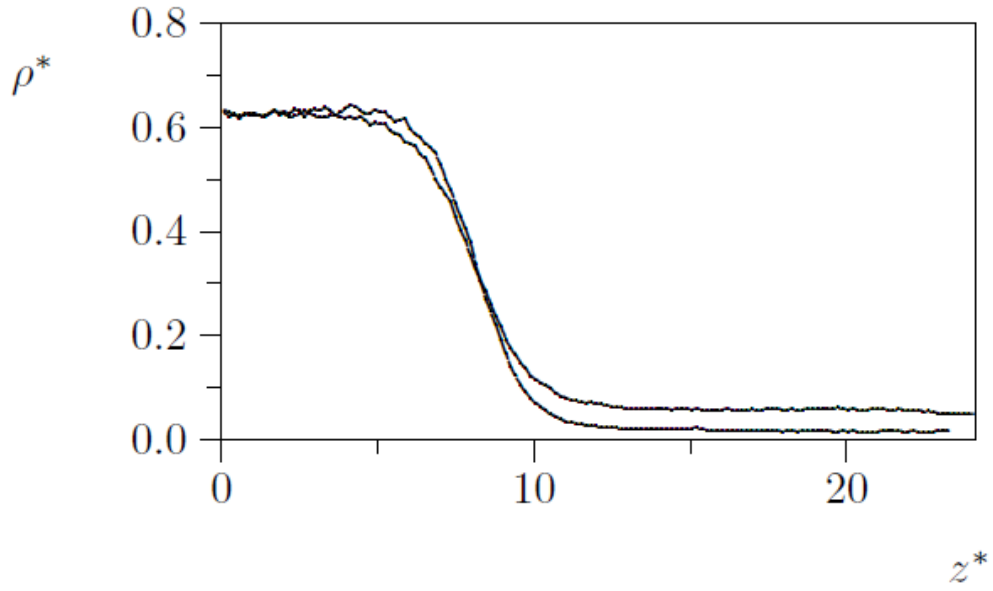

Fig. 9.: Density profiles $\rho(z)$ for equilibrium conditions and for steady state evaporation into vacuum at T_1 = 1.10. The profile with the weak maximum in the liquid and the lower vapour density is for evaporation from Run 7 and has been centred at the Gibbs dividing surface.

964 Fig. 10

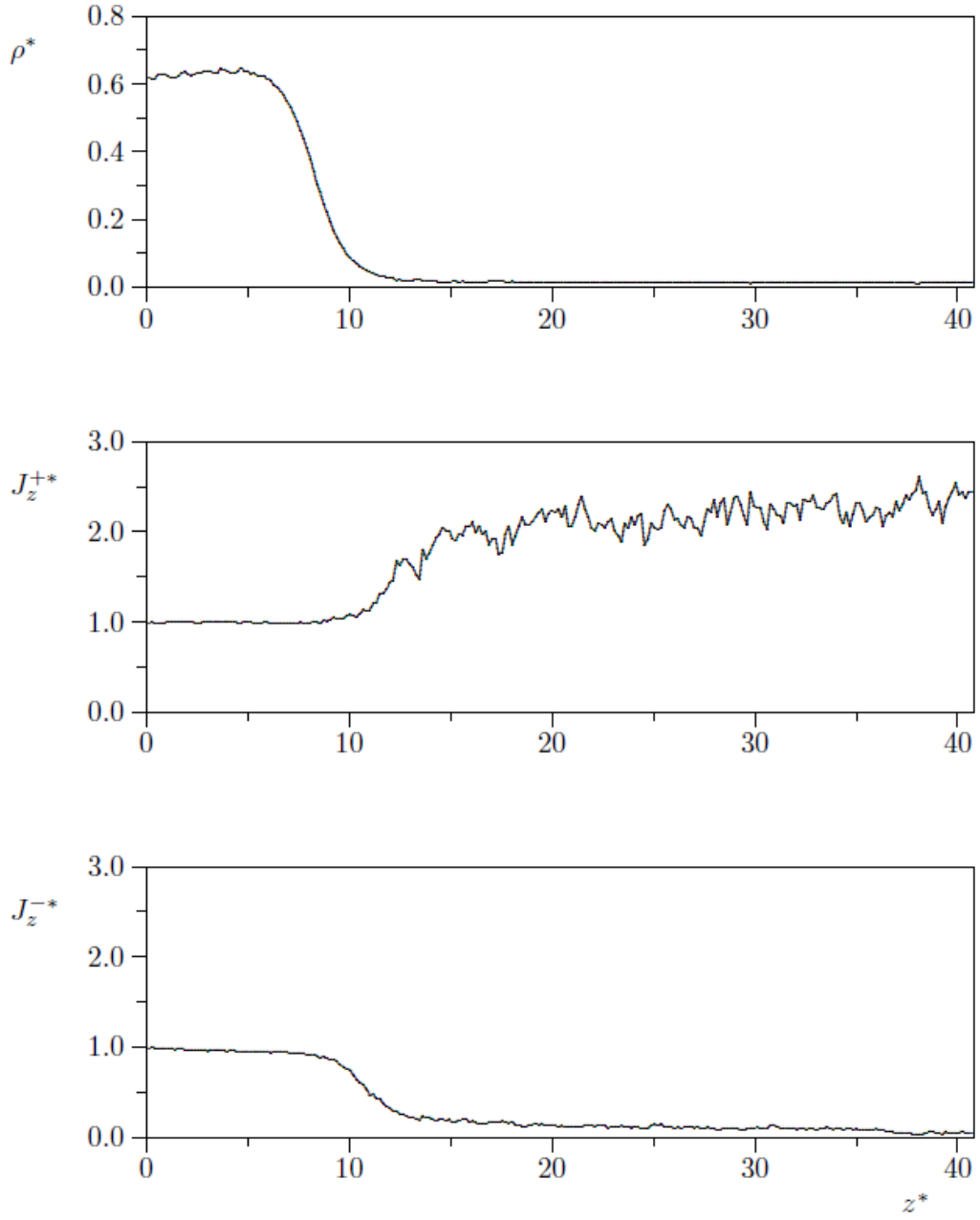

965

966 Fig. 10.: Evaporation into vacuum at T_1 = 1.10. NEMD profiles for the density ρ as well as

967 for the scaled outgoing and incoming particle fluxes J_z^+ and J_z^- from Run 9. The scaling was

968 made with respect to the Hertz flux at the local density $\rho(z)$ and the temperature T_1 according

969 to $J_z^+ = j_z^+/[\rho(z)(T_1/2\pi)]$.

970

971

972

Fig. 11

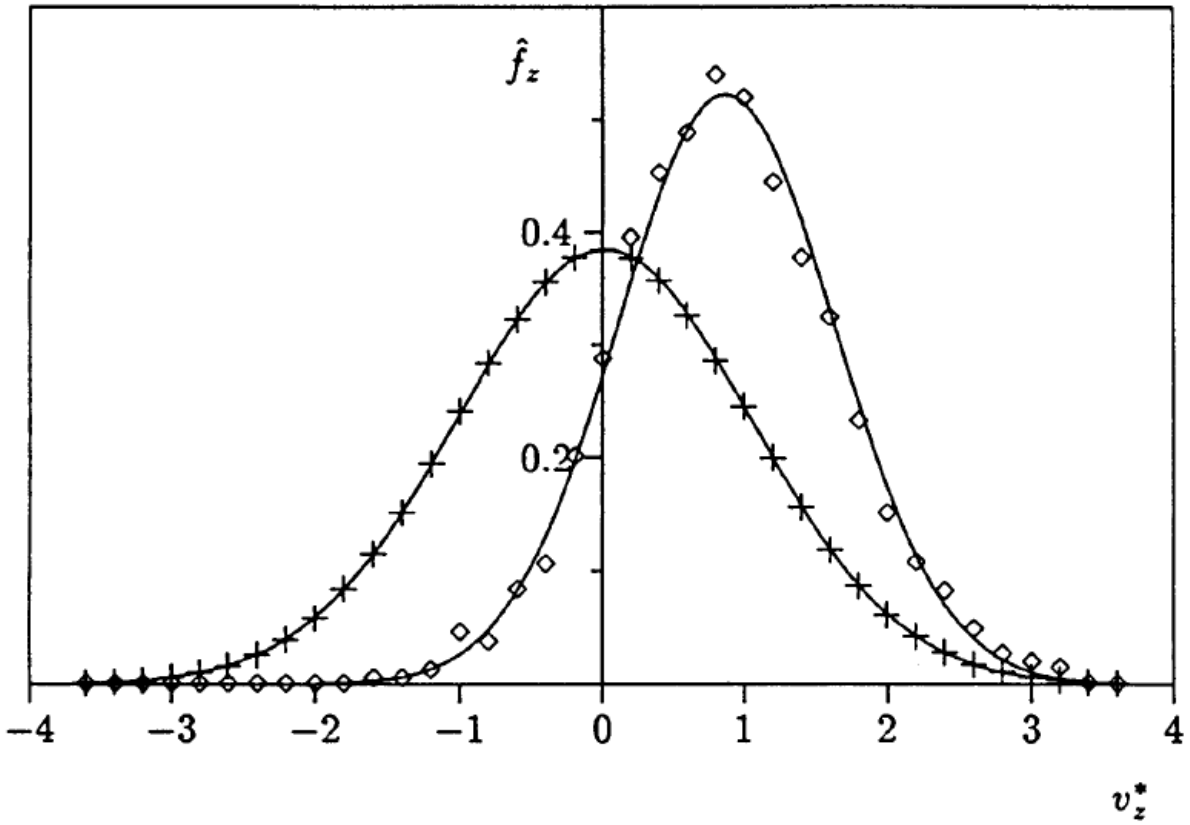

Fig 11: Contracted velocity distribution functions $\hat{f}_z$ for evaporation into vacuum at T_1 = 1.10. The crosses + denote data that were directly sampled by NEMD in the liquid, the diamonds ◊ denote data that were directly sampled in the vapour. The solid curves are Maxwellians according to Eq. (7) with temperatures and drift velocities for the liquid and the vapour as given in Table 1.

Fig. 12

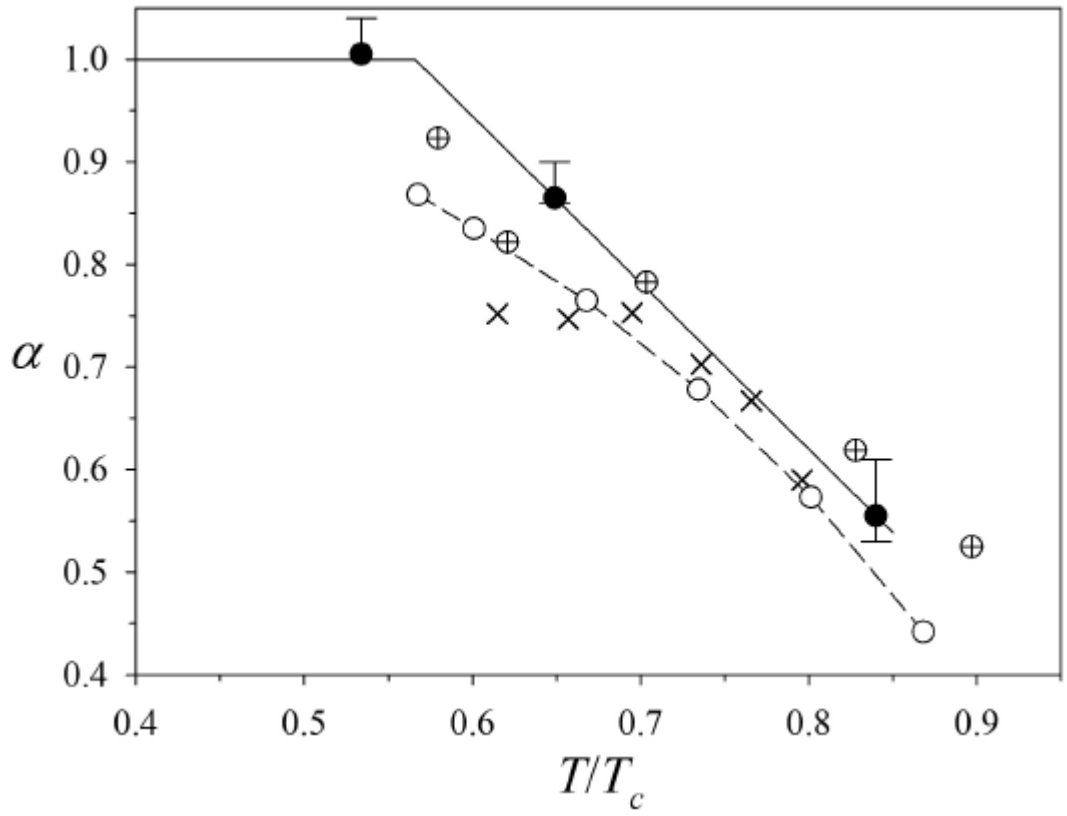

Fig 12: Evaporation coefficients α as a function of the reduced temperature T/T_c from the present NEMD simulations for full LJ • with uncertainties, from the correlation Eq. (31) ————, from the NEMD simulations for LJ3.5 of Anisimov et al. [19] ×, from the NEMD simulations for LJ4.4 of Ishiyama et al. [20] o with a guide for the eye - - - , and from the injection into equilibrium simulations for LJ3.5 of Tsuruta et al. [15] ⊕.

1009 **Table 1**: Parameters, auxiliary data and key results for nine NEMD runs for steady state
1010 evaporation into vacuum at the three temperatures T = 0.70, 0.85 and 1.10. The parameters are
1011 T_1, L_z, L_x and M. The auxiliary parameters are ρ', ρ'', λ, j_z^{+H} and c. The simulation results
1012 for temperature, density and drift velocity in the liquid are T_{le}, ρ_{le}, $v_{z,le}^D$ and in the vapour T_{ve},
1013 $T_{xy,ve}$, $T_{z,ve}$, ρ_{ve}, $v_{z,ve}^D$. The particle fluxes j_z^E and j_z^D were obtained from Eqs. (22) and (23).
1014 Derived quantities are λ, Kn and α.

	Run 1	Run 2	Run 3	Run 4	Run 5	Run 6	Run 7	Run 8	Run 9
T_l	0.70	0.70	0.70	0.85	0.85	0.85	1.10	1.10	1.10
L_z	46.2	46.2	77.2	47.3	47.3	78.8	48.3	48.3	81.6
L_x	10.3	10.3	10.3	10.5	10.5	10.5	10.7	10.7	10.7
M	100,000	120,000	150,000	100,000	75,000	75,000	50,000	50,000	30,000
T_{le}	0.70	0.70	0.70	0.85	0.84	0.85	1.09	1.08	1.09
ρ'	0.8426	0.8426	0.8426	0.7763	0.7763	0.7763	0.6410	0.6410	0.6410
ρ_{le}	0.836	0.836	0.836	0.769	0.771	0.769	0.625	0.627	0.625
$v_{z,le}^D$	0.0008	0.0009	0.0004	0.003	0.002	0.001	0.018	0.016	0.008
T_{ve}	0.53	0.53	0.55	0.63	0.61	0.59	0.73	0.70	0.67
$T_{xy,ve}$	0.65	0.64	0.67	0.76	0.72	0.67	0.80	0.74	0.70
$T_{z,ve}$	0.29	0.31	0.30	0.39	0.38	0.44	0.59	0.63	0.60
ρ''	0.00207	0.00207	0.00207	0.00966	0.00966	0.00966	0.05381	0.05381	0.05381
ρ_{ve}	0.0010	0.0010	0.0013	0.0041	0.0044	0.0036	0.019	0.021	0.015
λ	225	225	173	55	51	63	12	11	15
Kn	17	17	6.0	3.9	3.9	2.1	0.81	0.81	0.49
$v_{z,ve}^D$	0.67	0.71	0.64	0.75	0.72	0.76	0.66	0.59	0.84
j_z^E	0.00069	0.00070		0.0030	0.0031		0.013	0.012	
j_z^D	0.00068	0.00070	0.00083	0.0031	0.0031	0.0027	0.012	0.012	0.013
j_z^{+H}	0.00069	0.00069	0.00069	0.00355	0.00355	0.00355	0.02251	0.02251	0.02251
α	1.00	1.01		0.86	0.87		0.58	0.53	
c	0.94	0.94	0.96	1.02	1.01	0.99	1.10	1.08	1.06

1015

SUPPLEMENTARY MATERIAL

to

EVAPORATION FROM A FREE LIQUID SURFACE

AMAL LOTFI[1], JADRAN VRABEC[2] and JOHANN FISCHER[3]*

[1] *ista International GmbH, Grugaplatz 2, 45131 Essen, Germany,*

[2] *Lehrstuhl für Thermodynamik und Energietechnik, Universität Paderborn, 33098 Paderborn, Germany,*

[3] *Institut für Verfahrens- und Energietechnik, Universität für Bodenkultur, Muthgasse 107, 1190 Wien, Austria*

International Journal of Heat and Mass Transfer

This Supplementary Material contains figures with results from non-equilibrium molecular dynamics simulations of steady state evaporation from a free liquid surface at a low, a medium, and a high liquid temperature. These figures support the understanding of the results and conclusions in the main manuscript.

*Corresponding author. Tel.: +43-1-370 97 26-201; fax: +43-1-370 97 26-210

E-mail address: johann.fischer@boku.ac.at

Supplementary Figures to Section 4.1.: Evaporation at low temperature

Fig. S1

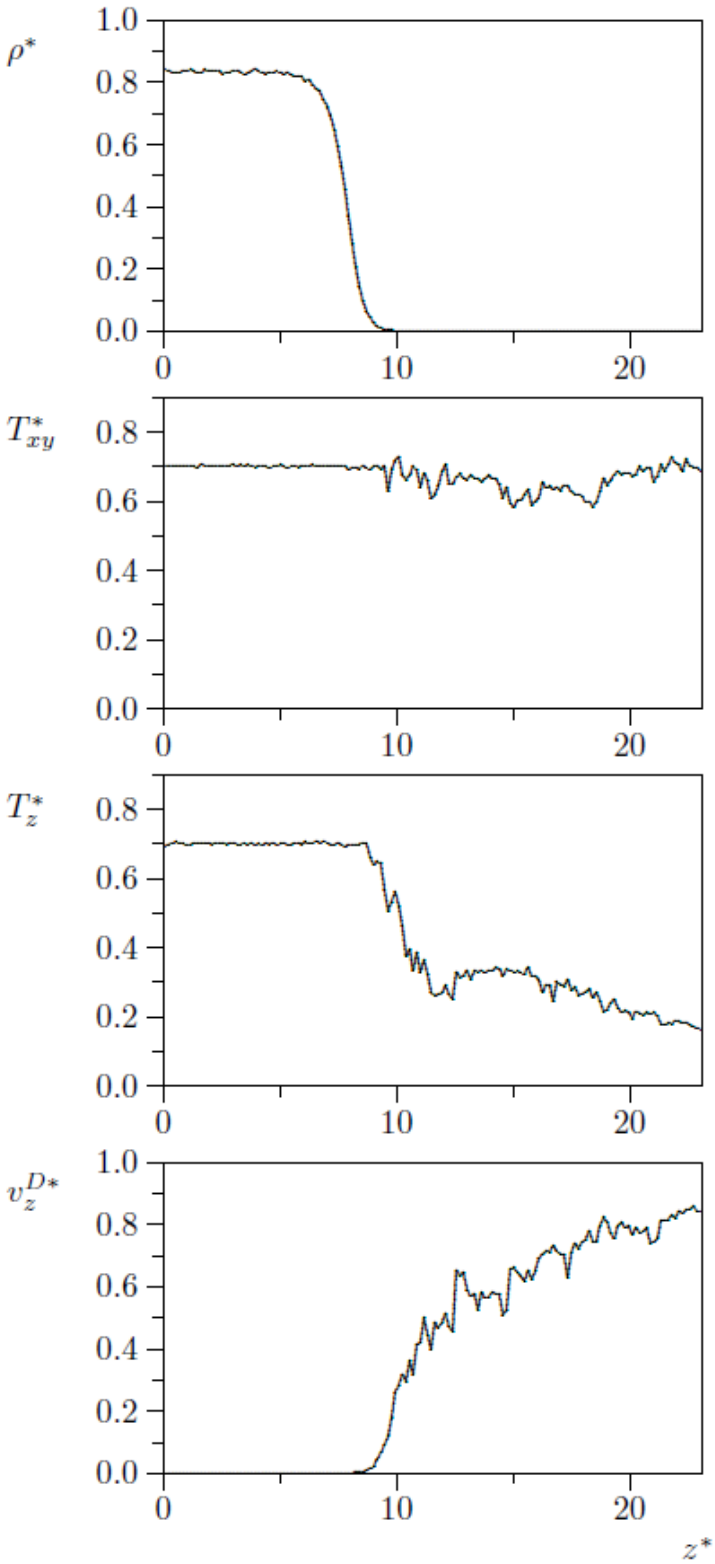

Fig. S1: Evaporation into vacuum at T_1 = 0.70. NEMD profiles for the density ρ, the temperature components T_{xy} and T_z and the drift velocity v_z^D up to $z = L_z/2$ from Run 1.

Supplementary Figures to Section 4.2.: Evaporation at medium temperature

Fig. S2

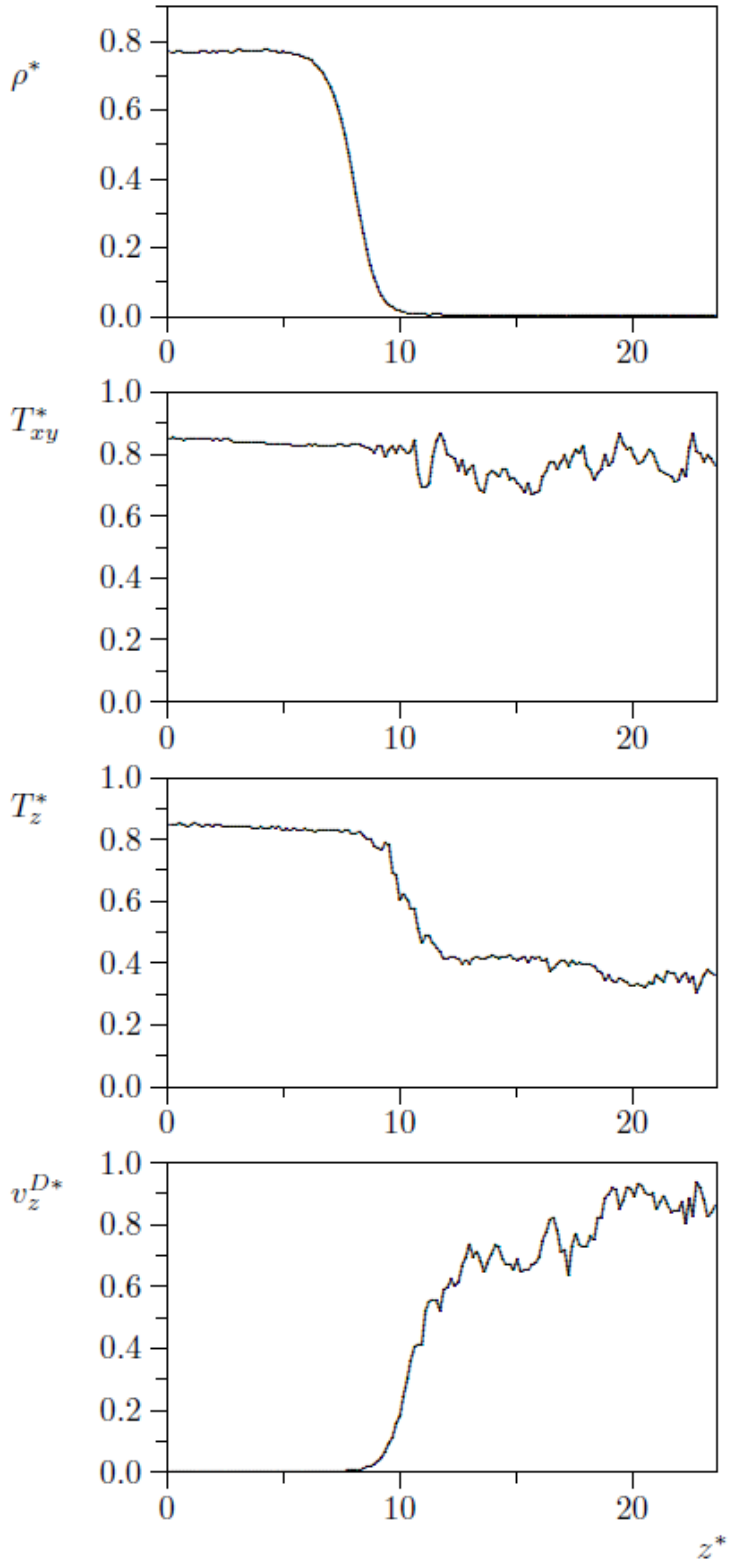

Fig. S2: Evaporation into vacuum at T_1 = 0.85. NEMD profiles for the density ρ, the temperature components T_{xy} and T_z and the drift velocity v_z^D up to $z = L_z/2$ from Run 4.

Fig. S3

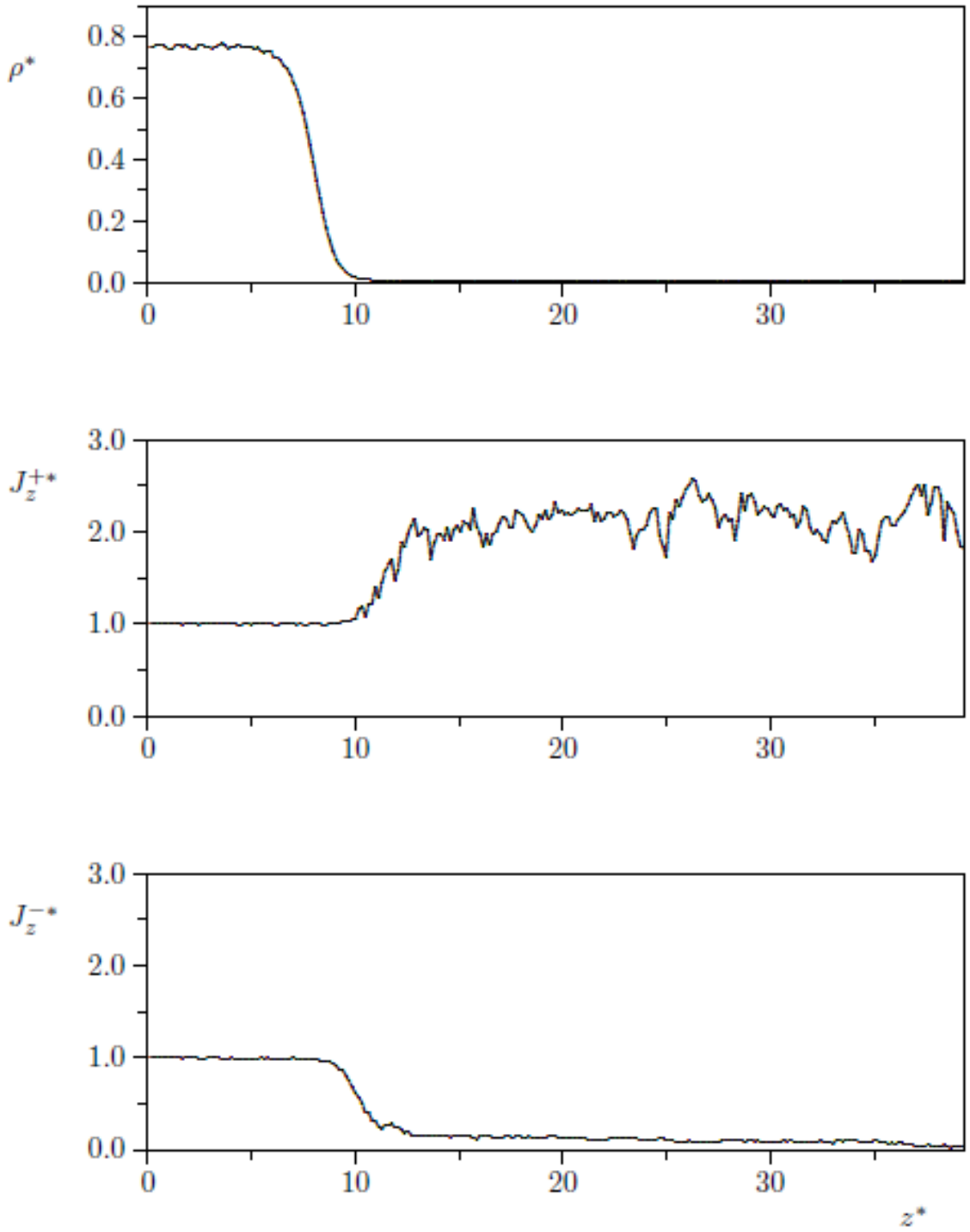

Fig. S3: Evaporation into vacuum at T_1 = 0.85. NEMD profiles for the density ρ as well as for the scaled outgoing and incoming particle fluxes J_z^+ and J_z^- from Run 6. The scaling was made with respect to the Hertz flux at the local density $\rho(z)$ and the temperature T_1 according to $J_z^+ = j_z^+/[\rho(z)(T_1/2\pi)]$.

Supplementary Figures to Section 4.3.: Evaporation at high temperature

Fig. S4

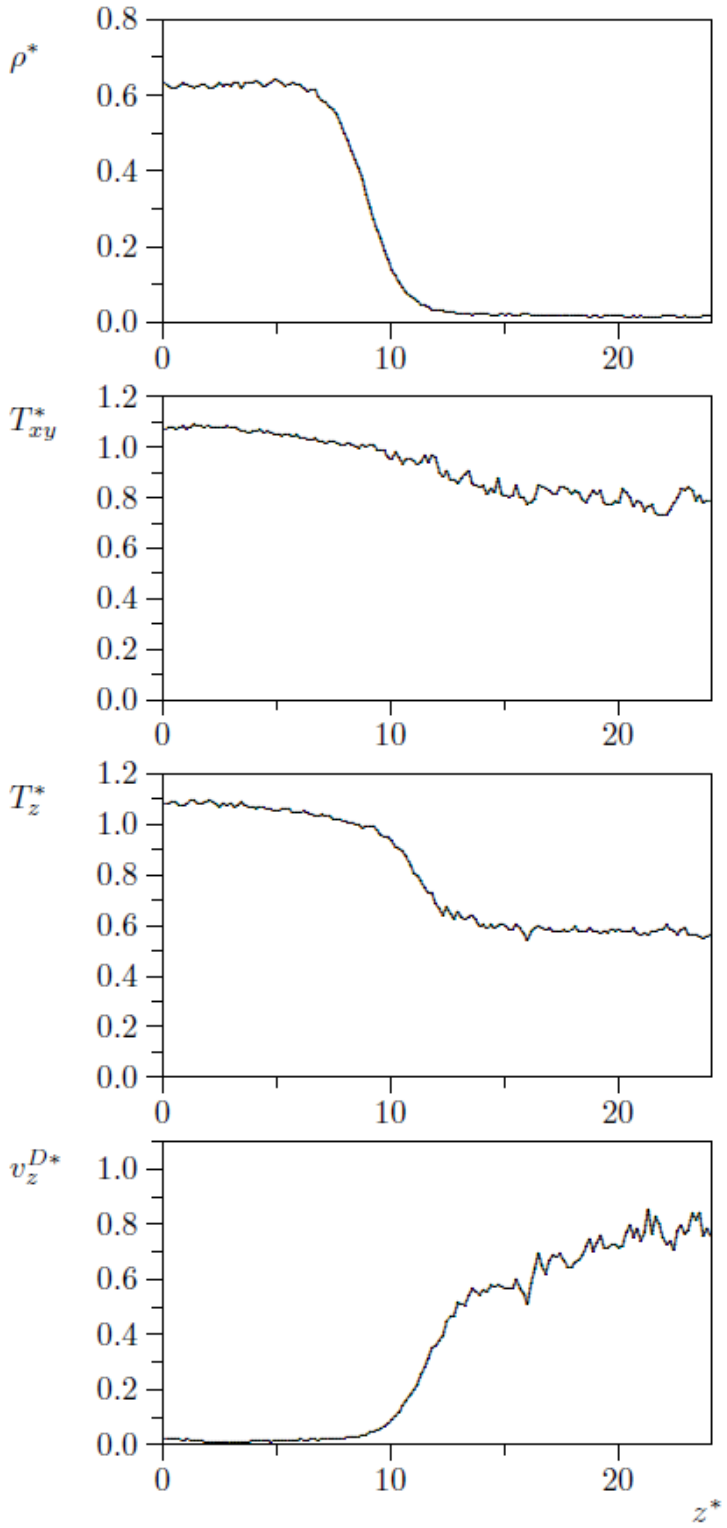

Fig. S4: Evaporation into vacuum at T_1 = 1.10. NEMD profiles for the density ρ, the temperature components T_{xy} and T_z and the drift velocity v_z^D up to $z = L_z/2$ from Run 7.

Fig. S5

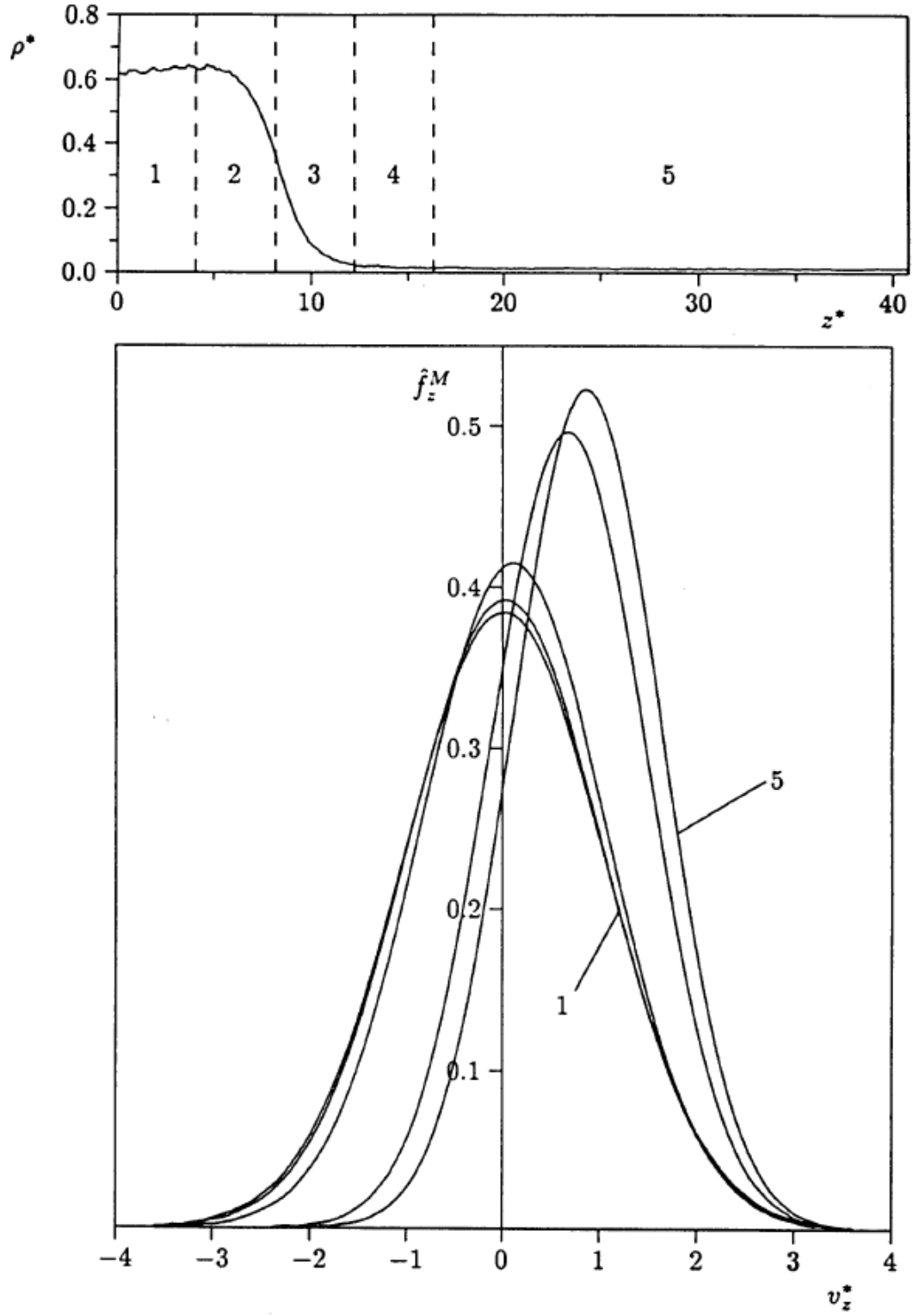

Fig. S5: Contracted Maxwellian distribution functions $\hat{f}_z$ according to Eq. (7) for steady state evaporation into vacuum at T_1 = 1.10 for different spatial regions shown in the upper part. The temperatures and drift velocities were taken as simulation averages of these regions.